The role of snow in controlling halogen chemistry and boundary layer oxidation during Arctic spring: A 1D modelling case study

Shaddy Ahmed[1], Jennie L. Thomas[1], Katie Tuite[2], Jochen Stutz[2], Frank Flocke[3], John J. Orlando[3], Rebecca S. Hornbrook[3], Eric C. Apel[3], Louisa K. Emmons[3], Detlev Helmig[4,5], Patrick Boylan[4], L. Gregory Huey[6], Samuel R. Hall[3], Kirk Ullmann[3], Christopher A. Cantrell[7,8], Alan Fried[4,9]

[1]Université de Grenoble Alpes, CNRS, IRD, Grenoble INP, IGE, Grenoble, France
[2]Department of Atmospheric and Oceanic Sciences, University of California, Los Angeles, CA, USA
[3]Atmospheric Chemistry Observations & Modeling Laboratory, National Center for Atmospheric Research, Boulder, CO, USA
[4]Institute of Arctic and Alpine Research, University of Colorado, Boulder, CO, USA
[5]Boulder A.I.R. LLC, Boulder, CO, USA
[6]School of Earth and Atmospheric Sciences, Georgia Institute of Technology, Atlanta, GA, USA,
[7]Department of Atmospheric and Oceanic Sciences (ATOC), University of Colorado, Boulder, CO, USA
[8]Laboratoire Interuniversitaire des Systèmes Atmosphériques (LISA), Creteil, France
[9]Earth Observing Laboratory, National Center for Atmospheric Research, Boulder, CO, USA

Key Points:

- A combination of factors including snow emissions, vertical mixing, and atmospheric chemistry explain surface Arctic halogen observations.
- Snow emissions of halogens impact atmospheric chemistry within a shallow layer near the surface.
- Surface HO_x concentrations are increased by up to a factor of 30 due to halogen chemistry.

Corresponding author: Shaddy Ahmed, `shaddy.ahmed@univ-grenoble-alpes.fr`

Corresponding author: Jennie Thomas, `jennie.thomas@univ-grenoble-alpes.fr`

Abstract

Reactive chlorine and bromine species emitted from snow and aerosols can significantly alter the oxidative capacity of the polar boundary layer. However, halogen production mechanisms from snow remain highly uncertain, making it difficult for most models to include descriptions of halogen snow emissions and to understand the impact on atmospheric chemistry. We investigate the influence of Arctic halogen emissions from snow on boundary layer oxidation processes using a one-dimensional atmospheric chemistry and transport model (PACT-1D). To understand the combined impact of snow emissions and boundary layer dynamics on atmospheric chemistry, we model Cl_2 and Br_2 primary emissions from snow and include heterogeneous recycling of halogens on both snow and aerosols. We focus on a two-day case study from the 2009 Ocean-Atmosphere-Sea Ice-Snowpack (OASIS) campaign at Utqiaġvik, Alaska. The model reproduces both the diurnal cycle and high quantity of Cl_2 observed, along with the measured concentrations of Br_2, BrO, and HOBr. Due to the combined effects of emissions, recycling, vertical mixing, and atmospheric chemistry, reactive chlorine is confined to the lowest 15 m of the atmosphere, while bromine impacts chemistry up to the boundary layer height. Upon including halogen emissions and recycling, the concentration of HO_x ($HO_x = OH+HO_2$) at the surface increases by as much as a factor of 30 at mid-day. The change in HO_x due to halogen chemistry, as well as chlorine atoms derived from snow emissions, significantly reduce volatile organic compound (VOC) lifetimes within a shallow layer near the surface.

1 Introduction

Halogen chemistry has a large impact on tropospheric chemistry in the polar regions (e.g., Abbatt et al., 2012; Barrie et al., 1988; Oltmans et al., 2012; Simpson et al., 2007, 2015; Steffen et al., 2008, 2013). Recently, new evidence of active Arctic chlorine chemistry has been attributed mainly to photochemical activation of chloride present in surface snow (Custard et al., 2017; Liao et al., 2014). Molecular chlorine (Cl_2) and nitryl chloride ($ClNO_2$), emitted from snow and aerosols, are sources of atomic chlorine (Cl) following their photolysis (McNamara et al., 2019). The highly reactive nature of Cl atoms makes it important even in trace amounts as Cl atoms react with volatile organic compounds (VOCs) up to three orders of magnitude faster than the more abundant hydroxyl radical (OH) (Atkinson et al., 2006). Active chlorine chemistry occurs simultaneously with reactive bromine chemistry each spring (e.g., Abbatt et al., 2012; Barrie et al., 1988; Simpson et al., 2007, 2015). The latter causes both ozone (O_3) and mercury depletion in the lowest part of the atmosphere (e.g., Oltmans et al., 2012; Steffen et al., 2008, 2013).

Halogens in the Arctic atmosphere ultimately originate from the ocean as halides (Cl^- and Br^-), which are activated on salty surfaces such as snow on sea ice, continental snow and aerosols (Abbatt et al., 2012). Chlorine and bromine species impact atmospheric chemistry within the polar boundary layer via reactions (R1)–(R9) (where X, Y = Cl or Br). Cl_2 photolyzes very quickly during the day (R1), with a photolysis lifetime of approximately 10 minutes, producing Cl atoms that rapidly react with ozone (R2) or VOCs (including methane) ((R3) and (R4)). Reactions (R3) and (R4) constitute the major reaction pathways of Cl atoms (Platt & Hönninger, 2003). This produces organic peroxy radicals (RO_2), including the methylperoxy radical (CH_3O_2), which ultimately contribute to hydroperoxyl radical formation (HO_2). HO_2 production, driven by chlorine chemistry, can impact HO_x chemistry ($HO_x = OH+HO_2$) by decreasing the OH/HO_2 ratio, as well as affecting the reactive bromine cycle. Molecular bromine (Br_2) is photolyzed very rapidly (photolysis lifetime $<$ 1 minute) to produce bromine atoms (Br) which can lead to efficient ozone destruction and formation of bromine monoxide (BrO). However, Br atoms react appreciably only with a few specific VOCs such as ethyne and the aldehydes and not with methane ((R3) and (R4) only occur for Cl). Br atoms can also

react with elemental mercury (Hg^0) to deplete near surface atmospheric levels and produce more reactive forms of mercury (Hg^{II}) (Steffen et al., 2008, 2013). Subsequent reaction of BrO with HO_2 forms HOBr (R5), which can be photolyzed to re-form Br and OH (R6). The net result of reactions (R5) and (R6) is the regeneration of a Br atom, which can facilitate further ozone depletion, and the conversion of HO_2 to OH, increasing the oxidative capacity of the atmosphere. At high BrO concentrations, Br_2 is also regenerated in the gas phase via self-reaction of BrO (R7).

$$X_2 \xrightarrow{h\nu} 2X \tag{R1}$$

$$X + O_3 \rightarrow XO + O_2 \tag{R2}$$

$$Cl + RH + O_2 \rightarrow RO_2 + HCl \tag{R3}$$

$$Cl + CH_4 \rightarrow CH_3 + HCl \tag{R4}$$

$$XO + HO_2 \rightarrow HOX + O_2 \tag{R5}$$

$$HOX \xrightarrow{h\nu} X + OH \tag{R6}$$

$$BrO + BrO \rightarrow Br_2 + O_2 \tag{R7}$$

Figure 1a highlights the typical diurnal behaviour of surface molecular halogen concentrations, snow emissions, solar radiation, and the boundary layer height observed during Arctic spring. Measured diurnal cycles of Cl_2 have shown a double-peaked profile, with peaks in the morning and late afternoon, followed by concentrations dropping below 0.8 parts per trillion by volume (pptv) after midnight (Custard et al., 2016; Liao et al., 2014; McNamara et al., 2019). At sunrise, increased solar radiation drives photochemistry within the snow interstitial air which leads to the release of halogens to the overlying atmosphere via diffusion and wind pumping (Bartels-Rausch et al., 2014; Grannas et al., 2007; Pratt et al., 2013; Thomas et al., 2011; Toyota et al., 2014). Boundary layer mixing modulates surface Cl_2 concentrations, with Cl_2 decreasing during the day due to a combination of its fast photolytic loss (R1) and the effects of boundary layer mixing. Solar heating of the lower atmosphere generates a well-mixed daytime boundary layer, mixes species away from the surface, and causes an increase in the boundary layer height (Anderson & Neff, 2008). Low light conditions (i.e., night and early morning) cause a reduction in the photochemical loss of Cl_2 (R1) and a collapse of the boundary layer. This effect has previously been demonstrated to drive evening increases of reactive nitrogen species ($NO_x = NO + NO_2$) at the surface in both the Arctic and Antarctic (Frey et al., 2015; Honrath et al., 1999, 2002; Thomas et al., 2011).

Figure 1b illustrates some of the key known emission sources of halogens from surface snow in the Arctic. Heterogeneous reactions involving hypohalous acids (e.g., HOCl and HOBr) (R8) and halogen nitrates (e.g., $ClONO_2$ and $BrONO_2$) (R9), have been recognized as a source of molecular halogens on halide-containing snow and aerosol surfaces (Aguzzi & J. Rossi, 1999; Deiber et al., 2004; Finlayson-Pitts et al., 1989; Hu et al., 1995; Pratte & Rossi, 2006). Bromine chloride (BrCl) is another product formed via reactions (R8) and (R9) on snow and aerosols, linking the chlorine and bromine chemical cycles. BrCl can then be photolyzed, re-forming Br and Cl atoms, as in reaction (R1).

$$HOX + X^-/Y^- + H^+ \xrightarrow{(surface)} X_2/XY + H_2O \tag{R8}$$

$$XONO_2 + X^-/Y^- \xrightarrow{(surface)} X_2/XY + NO_3^- \tag{R9}$$

At present, detailed descriptions of chlorine snow emissions remain absent from most 3D numerical models. Bromine mechanisms are included in some 3D models, but remain under discussion as to the source and recycling mechanisms involving snow (Falk & Sinnhuber, 2018; Fernandez et al., 2019; Herrmann et al., 2021; Marelle et al., 2021; Toyota et

al., 2011). Snow is a very complex photochemical medium and the release of halogens is determined by many uncertain processes/variables, including: snow physics; snow/ice chemistry (including photochemistry); gas transport within snow; and impurity concentrations and locations (Bartels-Rausch et al., 2014; Domine et al., 2008; Grannas et al., 2007; McNeill et al., 2012). As a result, modelling snow-covered environments using a first principles approach remains challenging and uncertain (Domine et al., 2013). Zero-dimensional box models are often used to study the effects of halogens on boundary layer chemistry under Arctic conditions (Custard et al., 2015; Liao et al., 2012, 2014; Piot & von Glasow, 2009; Thompson et al., 2015; Wang & Pratt, 2017). An inherent limitation of 0D models, however, is the absence of the vertical dimension necessary for simulating vertical transport and capturing concentration gradients in the atmosphere. Additionally, the physical conditions that characterize the polar regions (low temperatures, limited sunlight during winter, high albedo, etc.) can often create stable low-level temperature inversions resulting in shallow boundary layers (Kahl, 1990). This can greatly impact the vertical distribution of chemical species by acting as a barrier to vertical mixing and transport. One-dimensional models are therefore extremely useful tools which can include these processes to help us better understand the interactions between snow and the atmosphere (Cao et al., 2016; Herrmann et al., 2019; Lehrer et al., 2004; Piot & von Glasow, 2008; Thomas et al., 2011, 2012; Toyota et al., 2014; Wang et al., 2020).

The first observations of high Cl_2 levels within the Arctic boundary layer were reported in spring 2009, during the Ocean-Atmosphere-Sea Ice-Snowpack (OASIS) campaign at Utqiaġvik, Alaska (Liao et al., 2014). Cl_2 mixing ratios of up to 400 pptv were observed and an average noontime Cl-atom concentration of 2×10^5 atoms cm^{-3} was estimated from these observations. Daytime Cl_2 mixing ratios were highly correlated with sunlight and surface ozone levels (r^2 value = 0.86), indicating both are key requirements for Cl_2 production. Measurements of VOCs made during the campaign showed a clear impact of chlorine chemistry on VOC oxidation processes (Hornbrook et al., 2016). Measurement-derived estimates of Cl-atom concentration suggested the presence of a highly reactive surface layer, which led to an overprediction of VOC production and loss rates compared to the observations (Hornbrook et al., 2016). Interactions between radical chemistry, atmospheric mixing, and snow emissions need to be better understood in order to fully explain these observations and the impacts of halogens on boundary layer oxidation processes.

In this work, we address the following questions:

1. What combination of factors, including vertical mixing, snow emissions/recycling, and chemistry explain observations of halogens in the Arctic surface layer?
2. How are halogens vertically distributed within the polar boundary layer?
3. What is the impact of halogen chemistry on boundary layer oxidation processes as a function of altitude?

We answer these questions using an updated version of the Platform for Atmospheric Chemistry and vertical Transport in 1-dimension (PACT-1D) model (Tuite et al., 2021), which includes descriptions of halogen chemistry, emissions, and recycling. We compare our model with surface measurements of chemical species, including Cl_2 and Br_2, recorded during the 2009 OASIS campaign at Utqiaġvik, Alaska. In section 2, we introduce the measurements used from the campaign and the new model halogen updates are described in section 3. The model configuration used in this work is presented in section 4, followed by the model results and a discussion in section 5. Finally, the conclusions are presented in section 6.

2 OASIS 2009 campaign measurements

In this study, we use measurements taken during the OASIS campaign, which was conducted between March and April 2009 at Utqiaġvik, Alaska. Observations from this campaign were chosen due to the extensive chemical and meteorological measurements available, including direct measurements of Cl_2, Br_2, BrO, and a large number of VOCs. A summary of the measurements used in this study is given in Table 1 with the respective instruments/techniques used during OASIS. Meteorological measurements (temperature, winds, relative humidity) were made from two tower stations set up at the field site at several heights. At one of the tower stations, turbulent flux measurements were made using ultrasonic anemometers located at 4 heights (0.6 m, 1.8 m, 3.2 m, and 6.2 m above ground level (AGL)). Inorganic halogens (including Cl_2, Br_2, BrO and HOBr), as well as OH and HO_2, were measured using chemical ionization mass spectrometers (CIMS) at 1.5 m AGL (Hornbrook et al., 2011; Liao et al., 2011, 2012, 2014; Mauldin III et al., 1998; Tanner et al., 1997). Surface ozone and NO_x measurements were made using a chemiluminescence instrument on a second tower station, operated by the National Center for Atmospheric Research (NCAR), at 3 different heights (0.6 m, 1.5 m and 5.4 m AGL) (Helmig et al., 2012; Villena et al., 2011; Weinheimer et al., 1998). Additionally, measurements of formaldehyde (HCHO) made by a Difference Frequency Generation Tunable Diode Laser Absorption Spectrometer (Barret et al., 2011; Weibring et al., 2007, 2010), and 18 VOCs measured by a Trace Organic Gas Analyzer (TOGA) (Hornbrook et al., 2016) were made at these same heights. Carbon monoxide (CO) measurements were made using a CO infrared absorption analyzer (Parrish et al., 1994). Aerosol physical properties (size distribution and number concentration) were measured using an optical particle counter and two scanning mobility particle sizers (Woo et al., 2001). Finally, actinic flux measurements made by CCD Actinic Flux Spectroradiometers (CAFS) were used to calculate photolysis frequencies of 35 different reactions using a modified version of the Tropospheric Ultraviolet and Visible (TUV) radiation model version 4.4 (Madronich & Flocke, 1999; Shetter & Müller, 1999). Data from this campaign are available through the National Science Foundation (NSF) Arctic Data Center at `https://arcticdata.io/` (Apel, 2009; Cantrell, 2009; Fried, 2009; Guenther, 2009; S. R. Hall, 2009; Smith et al., 2009; Weinheimer, 2009).

3 Description of halogen chemistry within PACT-1D

The Platform for Atmospheric Chemistry and vertical Transport in 1-Dimension (PACT-1D) is the vertical column model used in this work to study Arctic halogen emissions and their impact on oxidation processes during the OASIS campaign. A full description of this model is given in Tuite et al. (2021). Chlorine and bromine gas-phase and heterogeneous reactions are added to this version of the model. Snow emissions and recycling mechanisms of chlorine and bromine have also been implemented and are described in the following sections.

3.1 Gas-phase and aerosol heterogeneous halogen chemistry

We update the existing PACT-1D mechanism to include additional chlorine and bromine gas-phase and heterogeneous reactions. The chemical mechanism in PACT-1D is based on the Regional Atmospheric Chemistry Mechanism version 2 (RACM2) (Goliff et al., 2013) using the Kinetic PreProcessor (KPP) (Sandu & Sander, 2006). The additional gas-phase bromine reactions are added following the implementation of Marelle et al. (2021) and are listed in the model chemical mechanism (Ahmed et al., 2021). Reactive and non-reactive heterogeneous uptake reactions of halogens on aerosols are also added to the model (Table 2). We track aerosol-phase chloride and bromide in the model by first initialising their concentrations to the chloride/bromide concentration in fresh sea salt aerosols. Second-order heterogeneous reactions consuming aerosol-phase halide

ions are treated as pseudo first-order reactions, following Marelle et al. (2021), maintaining mass conservation of each species.

3.2 Snow emission and recycling of Cl_2 and Br_2

Emissions of molecular halogens from snow have been identified as a key source of Arctic halogen production (Custard et al., 2017; Pratt et al., 2013). Solar radiation and ozone have both been reported as important factors that can regulate halogen emission fluxes from surface snow, with peak production under maximum irradiance and the presence of ozone (Liao et al., 2014; Liu et al., 2017). Halogen species deposited to the snow surface can also undergo recycling mechanisms to re-emit reactive halogens back into the atmosphere (Abbatt et al., 2012; Toyota et al., 2011). We therefore add four parameterizations to describe emissions of chlorine and bromine in this version of PACT-1D. We include (1) an emission of chlorine and bromine as a function of the available solar radiation and the surface ozone concentration, and (2) a recycling source of X_2 from the surface conversion of $XONO_2$ and HOX (where X = Cl, Br) on snow. In both cases, the exact parameterizations are determined by comparing modelled and observed halogen concentrations.

The emission of chlorine is parameterized as follows:

$$E_{\mathrm{Cl_2}}^{primary} = F_{(p,\mathrm{Cl})} \times (J_{\mathrm{Cl_2}})^{0.5} \times [\mathrm{O_3}] \tag{1}$$

$$E_{\mathrm{Cl_2}}^{recycling} = \gamma_{(snow,\mathrm{Cl})} \times (D_{\mathrm{ClONO_2}} + D_{\mathrm{HOCl}}) \tag{2}$$

where $E_{\mathrm{Cl_2}}^{primary}$ and $E_{\mathrm{Cl_2}}^{recycling}$ are the snow emission fluxes of Cl_2, $F_{(p,\mathrm{Cl})}$ is a correction factor which includes a scaling term and the height of the lowest model level (0.01 cm) in units of cm $s^{-\frac{1}{2}}$, $J_{\mathrm{Cl_2}}$ is the calculated photolysis rate of Cl_2, $[O_3]$ is the measured O_3 concentration (in molec cm^{-3}), $\gamma_{(snow,\mathrm{Cl})}$ is the probability of heterogeneous conversion on snow to re-form Cl_2 (between 0 and 1), and $D_{\mathrm{ClONO_2}}$ and D_{HOCl} are the model-calculated deposition rates of $ClONO_2$ and HOCl, respectively. In the case of primary chlorine emissions (equation (1)), different values of $F_{(p,\mathrm{Cl})}$ were tested in order to reproduce the Cl_2 measurement data in the model (Figure S1). Observed ambient concentrations of Cl_2 slowly increase in the morning, peak at solar noon, and decline into the evening hours. The best-fit primary emission flux for chlorine is found to be a function of $J_{\mathrm{Cl_2}}$ to the power of 0.5, with $F_{(p,\mathrm{Cl})} = 0.2$ cm $s^{-\frac{1}{2}}$. It is also well known that $ClONO_2$ and HOCl are converted on ice surfaces to re-form Cl_2 (IUPAC, 2009). However, within snow there are a number of complex physical and chemical processes that make these recommendations not directly applicable for snow. We therefore performed a series of sensitivity tests varying $\gamma_{(snow,\mathrm{Cl})}$ between 0 and 1, and found the best fit value of 0.1 for chlorine recycling on snow (Figure S2).

For bromine, the emission sources are described as:

$$E_{\mathrm{Br_2}}^{primary} = F_{(p,\mathrm{Br})} \times J_{\mathrm{Br_2}} \times [\mathrm{O_3}] \tag{3}$$

$$E_{\mathrm{Br_2}}^{recycling} = \gamma_{(snow,\mathrm{Br})} \times (D_{\mathrm{BrONO_2}} + D_{\mathrm{HOBr}}) \tag{4}$$

where $E_{\mathrm{Br_2}}^{primary}$ and $E_{\mathrm{Br_2}}^{recycling}$ are the snow emission fluxes of Br_2, $F_{(p,\mathrm{Br})}$ is a correction factor which includes a scaling term and the height of the lowest model level (0.01 cm) in units of cm, $J_{\mathrm{Br_2}}$ is the calculated photolysis rate of Br_2, $\gamma_{(snow,\mathrm{Br})}$ is the heterogeneous conversion efficiency on snow to re-form Br_2 (between 0 and 1), and $D_{\mathrm{BrONO_2}}$ and D_{HOBr} are the model-calculated deposition rates of $BrONO_2$ and HOBr, respectively.

For bromine, we found that the observations of bromine species are best described using primary emissions (equation (3)) as a function of $J_{\mathrm{Br_2}}$, with $F_{(p,\mathrm{Br})} = 0.01$ cm (equivalent to the lowest model level height and a scaling factor of 1). The conversion of $BrONO_2$ and HOBr on ice to re-form Br_2 is known to be more efficient than for chlorine (IUPAC, 2009), which in part facilitates the well known bromine explosion chemistry (Abbatt et al., 2012). We tested a range of possible conversion efficiencies for these reactions and found $\gamma(snow, \mathrm{Br}) = 0.6$ best reproduces the observations (Figure S3). For both equations (2) and (4), it is assumed that there is an infinite supply of Cl^- and Br^- in the snow. We do not include conversion of N_2O_5 on snow to form reactive bromine and chlorine due to the low NO_x concentrations compared to urban conditions.

There are large uncertainties in describing both the primary emission flux (equations (1) and (3)) from land-based snow, as well as the recycling of both bromine and chlorine species on snow (equations (2) and (4)), which must be considered in future work that use or further refine these parameterizations. First, there are significant uncertainties in vertical transport near the snow surface and in the lowest portion of the atmosphere (∼below 10 m). Therefore, as future work refines our knowledge of these vertical transport processes, we will need to revisit the values used for $F_{(p,\mathrm{Cl})}$, $F_{(p,\mathrm{Br})}$, $\gamma_{(snow,\mathrm{Cl})}$ and $\gamma_{(snow,\mathrm{Br})}$. In addition, descriptions of halogen emissions from land-based snow within 3D models remain limited. Bromine emissions triggered from ozone deposition to snow on sea ice is the main process considered by the bromine emissions/recycling scheme of Toyota et al. (2011). Here, we use ambient ozone concentrations rather than ozone deposition as the trigger for both bromine and chlorine on land-based snow, as suggested from observations. Our equations can be re-formulated as a function of the ozone deposition rate (which is directly dependant on ozone concentration) to be more consistent with equations proposed for snow on sea ice. Finally, production of BrCl from Arctic snow has been measured following irradiation of the snowpack, with multiphase reactions on snow also predicted to be significant contributors of BrCl production (Custard et al., 2017; McNamara et al., 2020). However, flux estimates of BrCl from snow remain uncertain and measurements of BrCl were not available during our selected simulation period (see section 4.1). We therefore only include BrCl production via heterogeneous reactions on aerosols (Table 2), but, this must be updated in future work to also include BrCl emissions from continental snow.

4 Model setup

4.1 Selection of OASIS simulation period

The model was set up for the dates of 18−19 March 2009 during the campaign; these dates were selected due to the high Cl_2 concentrations recorded and the limited influence from local pollution sources (Figure S4). The average daytime (06:00-20:00) Cl_2 mixing ratio for the two days was 59 pptv and surface ozone levels remained above 10 parts per billion by volume (ppbv), indicating that there was not a major ozone depletion event during this period. Average background levels of NO_x and CO over the entire campaign were recorded at ∼ 84 pptv and ∼ 160 ppbv, respectively (Villena et al., 2011). Measurements of NO_x and CO between 18−19 March do not suggest polluted conditions, with CO levels close to the average background measurements and influence from nearby anthropogenic sources likely to be minimal during this period. This is also consistent with the wind directions arriving at the measurement site, originating from the Arctic Ocean (north through northeast) for most of 18 and 19 March. Considering these criteria, the period between 18−19 March best met the requirements for our modelling case study.

4.2 Model configuration

We set up the vertical model grid (Figure 2a) using a total of 112 levels, with a logarithmic spacing for the lowest 1 m of the grid down to a lower boundary of 1×10^{-4} m. The model levels are linearly spaced up to 100 m, by 1-m increments, followed by a non-linear spacing to an upper boundary of 3000 m. This highly resolved vertical model grid allows us to analyse the impacts of halogen emissions on chemistry very close to the surface.

The 1D model is driven by input data obtained from the measurements (where possible), model output data and calculated explicitly from parameterizations. The atmospheric dynamics (temperature, pressure, relative humidity) are calculated using the 3D Weather Research and Forecasting (WRF) meteorological model (Skamarock et al., 2019) for Utqiaġvik, Alaska, and used to drive the 1D model physics in combination with the OASIS ground measurements. We use a WRF set up specifically optimised for the Arctic, described in Marelle et al. (2017), with the model domain centered at Utqiaġvik (domain shown in Figure 2b). A horizontal resolution of 25 km × 25 km is used with a vertical resolution of 50 levels, up to a pressure of 50 hPa. To validate the use of the WRF simulated meteorology, we compare WRF calculated temperatures at Utqiaġvik with surface measurements from OASIS and available vertical temperature profiles in Figure 3. The Integrated Global Radiosonde Archive (IGRA, Durre et al. (2006)) provides radiosonde data twice a day at 00:00 and 12:00 UTC (15:00 and 03:00 AKST, UTC-9, respectively) which we use to compare with our model results. Figure 3 shows that we are able to obtain very good agreement of both the surface and vertical temperature profiles in WRF compared to the observations.

The eddy diffusion coefficients (K_z) in the model are calculated following the parameterization described in Cao et al. (2016) and used in Herrmann et al. (2019). We calculate these values as measurement data of eddy diffusion coefficients during this period were sparse. Vertical K_z profiles are calculated using the measured friction velocities (u_*) at 1.8 m AGL, with the estimated surface inversion height (SIH) derived from the tower turbulent flux measurements. A comparison was made between the calculated K_z values and the available measurement data which showed that calculated values were approximately a factor of 3 greater than the observations. Above the surface inversion layer, we assume a fixed value of $K_z = 1$ cm^2 s^{-1}, following Cao et al. (2016). In our model runs, we calculate the SIH using a description based on eddy viscosity scaling, following equation (5) (Zilitinkevich et al., 2002; Zilitinkevich & Baklanov, 2002):

$$\mathrm{SIH} = C_s^2 (u_* L / |f|)^{0.5} \tag{5}$$

where C_s is an empirical constant (estimated as 0.7), u_* is the measured friction velocity, L is the calculated Obukhov length from the measurements and f is the Coriolis parameter (equal to 1.38×10^4 at the latitude of the study site).

Chemical concentrations in the model are initialised using both observations and CAM-chem model data (Buchholz et al., 2019; Emmons et al., 2020). Aerosol surface area and number concentration are fixed to the observations for the duration of the run throughout the boundary layer. To supplement the 35 reactions reported in the CAFS data set, additional photolysis rates were added using the TUV radiation model (version 5.0). Each of these additional rates is scaled to the reported NO_2 photolysis rate (J_{NO_2}). Chemical emission of NO_2 is also included in the model and is scaled as a function of J_{NO_2}. These emissions are added to the lowest model level, to simulate photochemical production from snow, and scaled to align with the NO_x levels measured during the simulation period. The 24-hour average NO_2 emission flux we use is 1.71×10^{13} molecules m^{-2} s^{-1}, in reasonable agreement with previous Arctic NO_x flux measurements

(Honrath et al., 2002). All input data are provided on 15 minute time resolution and the model is run using a 20-second time step.

5 Results and discussion

We study the impact of halogen emissions on oxidation processes during OASIS by performing the following model runs: a reference simulation without halogen emissions from snow (NOSURF); a model run with surface snow emissions and recycling of halogens active (BASE); and several sensitivity runs (FIXO3, AERO, PBLH). The model runs are summarised in Table 3 and are discussed in detail in the following section. In all model runs, we include heterogeneous chemistry on aerosols, which participates in active recycling of halogen species in all cases. We present the results and discussion in seven sub-sections. First, we present the meteorological conditions at the measurement site during the modelled period (section 5.1), followed by an analysis of the NOSURF (section 5.2) and BASE runs (section 5.3). We discuss in detail the results of the sensitivity tests performed (section 5.4), the influence of snow emissions on the vertical extent of halogen concentrations (section 5.5) and a comparison of the snow emission fluxes with other estimates (section 5.6). Finally, we analyse the impacts on boundary layer oxidation processes (section 5.7).

5.1 Meteorological conditions and air mass history

The measurements during OASIS were made approximately 5.5 kilometres northeast of Utqiaġvik, Alaska, near the Arctic Ocean (Barret et al., 2011; Boylan et al., 2014; Helmig et al., 2012; Hornbrook et al., 2016; Liao et al., 2012, 2014; Villena et al., 2011). Figure 4a and 4b show the sea ice concentration and snow cover, from satellite data, over Northern Alaska and locally near Utqiaġvik on 19 March 2009. Sea ice concentration data were obtained from the Advanced Microwave Scanning Radiometer for EOS (ASMR-E) on the NASA Aqua satellite (Melsheimer & Spreen, 2020; Spreen et al., 2008), and daily snow cover data from MODIS/Terra (D. K. Hall & Riggs, 2021). During March, the sample location was snow covered and the surrounding ocean largely covered by sea ice, typically reaching its annual maximum in spring. These conditions can influence the chemical composition of the arriving air mass at the measurement site via surface emissions and subsequent atmospheric chemistry. Meteorological conditions, such as wind speed, wind direction and surface temperature, can also alter surface chemical concentrations via impacts on boundary layer dynamics. Winds on both days were recorded arriving from the northeast, over the Beaufort Sea, carrying clean air masses to the measurement site. During this period, wind speeds were moderate to weak (< 5 m s^{-1}), lower than much of the campaign period, and surface temperatures were close to the March average. A strong low-level temperature inversion was also observed for the duration of these two days, indicating stable boundary layer conditions, which is likely to inhibit vertical mixing of species between the inversion layer top and the overlying atmosphere.

We use the regional meteorological model WRF (setup described in section 4.2) to both drive the 1D model atmospheric physics and to understand the regional meteorological conditions during the sampling period. Simulated 2-m temperature and 10-m winds over Northern Alaska are shown in Figure 4c and 4d on 18 and 19 March 2009 (local noon) respectively. The wind direction from WRF on both days captures the northern/northeasterly winds measured at the site, as well as the weaker wind speeds on 19 March. This analysis allows us to next identify the origin for air arriving at the measurement site, using the Lagrangian particle dispersion model, FLEXPART-WRF (Brioude et al., 2013). FLEXPART-WRF is driven by the meteorological conditions simulated by WRF and is run in backward mode to simulate air mass histories for the modelled period. These simulations are performed by releasing a total of 100,000 air parcels at the time when Cl_2 maxima were observed for each day (10:00 and 18:00 local time for 18 and 19 March, respectively) and

run backwards in time for 6 hours. Figures 4e, 4f, 4g and 4h show the calculated surface (0−100 m) potential emission sensitivities (PES) near Utqiaġvik. The PES indicates the length of time the air mass is sensitive to surface emissions for each FLEXPART-WRF model grid box. In Figure 4e and 4f, we show that air masses on these days were unaffected by either the town of Utqiaġvik or Prudhoe Bay (southeast of Utqiaġvik). Transport of air masses over sea ice may impact the halogen concentrations measured at the site. However, due to the relatively short lifetimes of Cl_2 and Br_2, these species would be photolytically destroyed over land-based snow and we assume that local snow emissions provide the main source of Cl_2 and Br_2 for our case study (see section 5.2).

5.2 Model results without snow emissions or recycling

A model simulation without halogen emissions from snow or surface recycling (NO-SURF) was first performed as a reference simulation. The results from this simulation are compared to measured species at 1.5 m AGL in Figure 5 (blue curve). The halogen species (Cl_2, BrO, and HOBr) in this simulation remain negligible for the duration of the simulation, with the exception of Br_2 which is initialised as described below, showing that additional sources of both chlorine and bromine are required to explain the observations. Surface Br_2 is initialised to the average midnight value (15 pptv) that was recorded during OASIS (Liao et al., 2012), which fell rapidly to zero after 08:00 on the first day, indicative of photochemical loss. No significant levels of Br_2 after this period are modelled, suggesting that bromine recycling solely on aerosols is not efficient enough to replenish measured levels of Br_2 and other bromine species. Local snow emissions of Br_2 are therefore necessary to replenish bromine levels during the simulation period.

Surface measurements of both NO and NO_2 were higher than the background average ($\sim$ 82 pptv), reaching daytime peaks of close to 250 pptv. These measurements were likely impacted by both local background NO_x emissions from snow (Honrath et al., 1999, 2002) and transient point sources. We filtered out the extreme elevated point sources of pollution (above 500 pptv), and use an hourly average of NO and NO_2 concentrations to smooth out sharp peaks arising from local point sources. The observations (Figure 5e and 5f) show some remaining sharp peaks of NO_x on both days, likely caused by these local emission sources, which are difficult to estimate. In addition, a large increase of NO_2 on the evening of 19 March was recorded, corresponding with a change of wind direction and air mass, bringing air from more polluted regions to the measurement site. Stable conditions and low wind speeds may have also facilitated the build-up of higher NO_x concentrations near the surface on these two days. The impact of these local point sources, and of advected polluted air masses, are therefore difficult to simulate in the model to represent the true NO_x concentrations observed at the measurement site. Modelled values reach and even exceed the measured daytime peaks, with a large overestimation in NO on day 2, before falling to lower than 100 pptv at night. The low concentration of modelled halogens would certainly contribute to the overestimation of NO_x concentrations via halogen oxide limited reactions with NO and NO_2. Changes in the surface ozone levels over the two days are not fully captured by either the NO-SURF or BASE simulations; this is possibly due to horizontal advection of air masses, affecting ozone levels measured at the site, which is not included in our model runs. Finally, we find a general underestimation of both HCHO and HO_2 levels, indicating missing oxidants and oxidation chemistry, and a predicted midday OH concentration between $0.7 - 1.5 \times 10^6$ molecules cm^{-3} for the two days.

5.3 Model results with halogen emissions from snow and surface recycling

When snow and recycling emissions of halogens are active (BASE run), we obtain much better agreement with the measured surface mixing ratios compared to the NO-SURF run. Measured Cl_2 levels reached up to 150 and 300 pptv on 18 and 19 March 2009

respectively (10 minute average). Figure 5 (red curve) shows the model performs well, capturing both the timing and intensity of the morning and late afternoon Cl_2 peaks on the first day, with some discrepancies on day 2. Early morning increase of Cl_2 was recorded after sunrise, suggesting a photochemical production mechanism, which is captured by the model on both days. Daytime levels of modelled Cl_2 on day 2 are overpredicted, by up to 100 pptv, with the difference possibly explained by weak vertical mixing and a shallow daytime boundary layer. The effects of this on surface chemical concentrations are discussed in more detail in section 5.5. Nighttime Cl_2 mixing ratios fall to near-zero levels in the model, which is consistent with the measurements on both days. Our model results show that the nighttime (20:00-06:00) reduction of Cl_2 at 1.5 m is largely explained by depositional loss to the ground (see section 5.5). Together, vertical transport and deposition represent the dominant nighttime loss processes ($\sim 94\%$) for Cl_2 at 1.5 m. Heterogeneous uptake of Cl_2 on aerosols and reaction with bromide has also been suggested as a potential Cl_2 sink (and a source of BrCl) (Hu et al., 1995; Wang & Pratt, 2017). We find that the reaction of Cl_2 with bromide on aerosols accounts for nearly 5% of nighttime removal of Cl_2 at 1.5 m, which comprises the majority (95%) of the nighttime chemical loss for Cl_2.

Modelled bromine species (Br_2, BrO, and HOBr) are also in close agreement with the measurements, with a slight underestimation of BrO and HOBr on day 1. Daytime measurements of Br_2 on these two days are missing due to unstable background Br_2 measurements that led to observations below the detection limit (2.0 pptv) (Liao et al., 2012). We find that modelled daytime levels of Br_2 are close to this 2 pptv detection limit, due its very fast photochemical loss. At night, we find an accumulation of the photolabile Br_2, via the surface recycling mechanism, which provides reactive bromine for the following day. This is consistent with the average diurnal profile measured for Br_2 during OASIS (Liao et al., 2012), as well as other Arctic measurement campaigns during spring (McNamara et al., 2020; Wang et al., 2019). Modelled BrO and HOBr diurnal profiles are also in agreement with the observations, with peaks at noon on the first day, indicative of production via Br atoms, and near zero at night. On day 2, a second peak for both BrO and HOBr is recorded in the late afternoon, coinciding with the evening peak of Cl_2. This suggests that the second peak in halogen species could possibly be due to a change in the boundary layer meteorology (e.g., collapse of the boundary layer) rather than chemical production.

The model captures the general trend of NO_x and we obtain better agreement with the observations in the BASE run, however, the model does not capture some peaks which may be due to advection of more polluted air masses (e.g., evening of 19 March) or transient point sources. Simulated NO_x levels are highly affected by the presence of halogen emissions, with both NO and NO_2 levels reduced in the BASE run compared to NOSURF. Halogens can react with NO_x to produce halogen nitrites and nitrates (e.g., $ClNO_2$, $ClONO_2$, $BrONO_2$), which act as an important reservoir to sustain reactive halogen chemistry. These species can release halogens back into the atmosphere either directly via photolytic destruction, or by chemical reactions on aerosols and surface snow. O_3 levels in the BASE run also show a steady decline over the two days, with O_3 changes dominated by vertical mixing and deposition to the ground in our particular simulation period. Modelled HCHO and HO_2 levels are also in better agreement with the observations following the addition of halogen emissions. We find an increase in the daytime HO_x ($HO_x = OH+HO_2$) levels by roughly $20-30$ times compared to the NOSURF run, indicating much more active HO_x chemistry, which can be attributed to halogen chemistry. Overall, we show that halogen emissions from snow and snow-surface recycling are necessary to reproduce surface concentrations of several key species measured during OASIS, with a considerable impact on HO_x concentrations and oxidative chemistry.

5.4 Model sensitivity runs

We investigate the effects of different model uncertainties on surface chemical concentrations by performing 3 sensitivity tests. The aim of these runs is to explore uncertainties in both the chemical and dynamical mechanisms in our model and their associated impacts on surface concentrations. We test whether changes in the modelled ozone concentration, halogen recycling on aerosols or vertical mixing can be adjusted to better explain the observations. Descriptions of the runs performed are included in Table 3 and are summarised here, followed by a discussion of the results compared with the surface observations (Figure 6).

1. **FIXO3**: We first address the impact of ozone on halogen concentrations by fixing the modelled ozone to the measurements within the boundary layer (Figure 6, green curve). Bromine levels in this run are greatly affected by the change in ozone availability due to the reaction with Br atoms (R2). On 18 March, BrO and HOBr are both underestimated in this run compared to the observations, followed by an overestimation on 19 March (when there was more ozone available). Nighttime Br_2 levels are underestimated by $\sim$ 10 pptv compared to the observations and BASE run, with this difference likely explained by the lower levels of BrO on day 1, resulting in less $BrONO_2$ formation and recycling to re-form Br_2. The daytime HO_2 concentration on day 2 is approximately 68% lower than the BASE run, due to increased BrO levels and subsequent loss via reaction (R5). The results from this run point to potential inaccuracies in the emission parameterizations of bromine, uncertainties in the downward mixing of ozone in the model from above the boundary layer, or, to the missing treatment of advected air masses, all of which require further exploration and testing.
2. **AERO**: To test whether heterogeneous recycling on aerosols could contribute a significant source of halogens, we increase the heterogeneous reactive uptake coefficients for Cl_2, Br_2 and BrCl formation reactions by a factor of 10 (Figure 6, magenta curve). This test fails to show significant changes to the halogen concentrations, indicating that recycling on aerosols contributes only a minor source of reactive halogens in our model runs. Interestingly, nighttime Br_2 levels fell by up to 5 pptv when compared to the BASE run, caused by lower $BrONO_2$ levels ($\sim$ 25% reduction) as it was more efficiently recycled on aerosols.
3. **PBLH**: We explore uncertainties in the boundary layer dynamics by testing a different expression to calculate the SIH from the meteorological measurements (Figure 6, orange curve). The expression used in this run (equation (6)) was originally developed for a stable mixed layer over the ocean by Pollard et al. (1973), and was found to also be applicable to the South Pole by Neff et al. (2008):

$$\mathrm{SIH} = 1.2u_*(fN_B)^{-0.5} \tag{6}$$

$$N_B = \sqrt{\frac{g}{T}\frac{\partial\theta}{\partial z}} \tag{7}$$

where u_* is the measured friction velocity, f is the Coriolis parameter (equal to 1.38×10^4 at the latitude of the study site), N_B is the Brunt-Vaisala frequency, g is the acceleration due to gravity, T is the absolute temperature and $\partial\theta/\partial z$ is the potential temperature gradient. This results in a SIH which is several metres greater than previously used for the BASE run (Figure S5), leading to some key differences in the modelled chemical species. Most notably, we see a reduction in daytime Cl_2 levels at 1.5 m, by up to 60 pptv, on day 2 compared to the BASE run due to an increased SIH. This shows how sensitive surface concentrations can be to small changes in the boundary layer conditions, with significant uncertainties in vertical transport near the snow surface and lower atmosphere. This is discussed in more detail in section 5.5.

In summary, these sensitivity tests show that modelled surface concentrations are influenced by a number of parameters, which require better understanding of specific processes in order to constrain halogen emissions. Changes in ozone and boundary layer dynamics (vertical mixing) had the largest impacts on halogen concentrations, as well as influencing surface NO_x and HO_x levels. We find that uncertainties in heterogeneous reactions on aerosols do not explain the underestimation of BrO and HOBr on day 1, and represent only a minor source contribution of halogens in our model case. Additional studies designed to investigate these processes and reduce known uncertainties for the Arctic region are needed to further evaluate the source contributions of halogens from snow.

5.5 Vertical influence of snow emissions and recycling on halogens

In this section, we use the BASE run to understand the vertical distributions of Cl_2 and Br_2 (Figure 7a and 7b respectively). No vertically resolved measurements were available for either species, therefore, no direct comparison can be made to the model results. We find that the majority of modelled Cl_2 (approximately 97%) is confined to the lowest 15 m of the atmosphere and rapidly decreases with altitude. This implies highly active chlorine chemistry at the surface. Very little Cl_2 is present above 15 m, indicating a strong vertical gradient in chemical reactivities, with the vertical distribution of Cl_2 influenced by the height of the surface inversion. During the campaign, the surface layer height ranged from as low as a few metres up to several hundreds of metres and was estimated to be very shallow (< 50 m) during the simulation period (Boylan et al., 2014). Low-level temperature inversions and shallow boundary layers are a common phenomena in cold polar regions and are frequently characterised by stable conditions and low wind speeds. Typically, solar heating of the surface generates a turbulent well-mixed daytime boundary layer, creating a larger volume in which chemical species can be distributed. This simultaneously increases the vertical transport of species away from the surface and results in decreasing concentrations of chemical species that would otherwise build up near the surface. The diurnal evolution of the surface layer can be seen following this behaviour on the first day but not on the second. We are therefore able to capture the daytime reduction in surface Cl_2 levels on day 1, following the morning peak, but overestimate Cl_2 levels on day 2. This high daytime Cl_2 concentration is simulated when the wind speed and estimated SIH were very low (< 1 m s^{-1} and < 10 m, respectively), confining Cl_2 to a very shallow layer close to the surface. The PBLH sensitivity test also shows similar behaviour of the surface layer on the second day, however estimated a SIH several metres higher during the day, resulting in a reduction of Cl_2 at this time (Figures S5 and S6). Differences in the SIH estimates between equations (5) and (6) are discussed in detail by Boylan et al. (2014), but further evaluation is beyond the scope of this study.

In Figure 7c and 7d, we plot the changes in concentration of Cl_2 and Br_2 due to transport and deposition, respectively. The change in both Cl_2 and Br_2 concentrations, due to vertical transport, is highest during the day following release from snow and transport into the atmosphere. During the night, Cl_2 is mainly transported downward to the surface and lost via deposition to the ground. Deposition in the model is calculated using an approach of molecular collisions with the ground and applying a non-reactive uptake probability (α) (Tuite et al., 2021). This allows us to calculate deposition of different species without prescribing a deposition velocity. For Cl_2, we set $\alpha = 5 \times 10^{-5}$, following the lower limit recommendation of Burkholder et al. (2019). On 19 March, transport of Cl_2 is clearly limited by the height of the inversion layer, with Cl_2 transport not exceeding more than 10 m altitude, thereby concentrating Cl_2 at the surface. Figure 7d shows that the upward transport of Br_2 is at its maximum during the day on 18 and 19 March. With no significant concentrations of Br_2 at higher altitudes, this indicates that daytime Br_2 is lost via its fast photolytic destruction. Vertically resolved measurements of halogens above the Arctic snow surface are highly desirable for further model evaluation and development.

5.6 Modelled halogen snow emission fluxes compared to observed estimates

Here, we compare the surface emission fluxes of chlorine and bromine estimated in this work to previous flux estimates. The model emission flux contributions of Cl_2 and Br_2 are shown in Figure 8a and 8b, respectively. Emission of both species peak at solar noon on each day, coinciding with maximum solar radiation at the snow surface, before falling to zero at night. This is consistent with previously reported halogen emission fluxes measured from the Arctic snowpack (Custard et al., 2017). During February 2014, snowpack flux estimates of Arctic Br_2 and Cl_2 were calculated, based on vertical gradient measurements, for the first time near Utqiaġvik. Estimates of these fluxes ranged between $0.7-12\times10^8$ and $0.02-1.4\times10^9$ molecules cm^{-2} s^{-1} for Br_2 and Cl_2, respectively. We modelled midday fluxes for chlorine of 4.3×10^9 and 7.2×10^9 molecules cm^{-2} s^{-1} for 18 and 19 March, respectively, with the primary photochemical snow emission mechanism the main contributor to chlorine emissions. This is several times higher than the values reported by Custard et al. (2017). This may be explained by increased available sunlight during March compared to February (when the flux measurements were made), enhancing halogen production. Additionally, ambient concentrations of chlorine were much lower in February 2014 than those measured in March 2009, with daytime values ranging between 5−20 pptv in February 2014 and 59 pptv for the simulation period. Both of these reasons would suggest higher snow emission fluxes of halogens between 18−19 March 2009 than estimated previously. Production of Cl_2 via snow surface recycling of HOCl and $ClONO_2$ was minimal over the two days, with almost no production of Cl_2 at night, which explains the difference in the nighttime concentrations of Cl_2 and Br_2. There are uncertainties to the efficiency of this recycling (see section 3.2), however, sensitivity tests showed no significant increase in Cl_2 when the recycling efficiency of these species was increased (Figure S2).

Modelled bromine emission fluxes at midday are calculated at 4.9×10^8 and 5.0×10^8 molecules cm^{-2} s^{-1} for 18 and 19 March, respectively, in close agreement with the range reported by Custard et al. (2017). Both primary photochemical and snow recycling emissions of bromine are important Br_2 production mechanisms and contribute significantly to the total Br_2 emission flux. Surface recycling of $BrONO_2$ is the main source of Br_2 on day 1, highlighting the influence of NO_x on bromine chemistry. This mechanism drives the accumulation of Br_2 at night, as this emission source remains significant later into the evening on day 1 compared to the primary snow emission, which falls to zero after sunset. Previous box modelling studies have shown that even under low NO_x levels (< 100 pptv), formation of $BrONO_2$ is significant (Liao et al., 2012; Thomas et al., 2012; Wang & Pratt, 2017), and under high NO_x levels (> 700 pptv) formation of both BrO and HOBr are suppressed, whereas the rate of $BrONO_2$ formation remained largely unaffected (Custard et al., 2015). Due to the difficulty of measuring $BrONO_2$, no measurements have yet been reported in the Arctic to the best of our knowledge. Future work remains to compare the partitioning of HOBr and $BrONO_2$ under different NO_x conditions.

5.7 Boundary layer VOC oxidation processes

We have shown (in section 5.3) that with the addition of halogen emissions (BASE run), we obtain good agreement with the measured HO_2 concentration at the surface and predict an increase in OH (Figure 5). To further understand the links between halogens, HO_x cycling and oxidative chemistry, we analyse the major HO_x production and loss reactions, as well as VOC chemical lifetimes with respect to OH and Cl. First, we compare the difference in modelled HO_x concentrations between the NOSURF and BASE runs, as well as the change in partitioning of OH/HO_2 between the two runs.

Figure 9a shows the modelled HO_x and Cl atom concentrations in the NOSURF and BASE runs at 1.5 m AGL. We see a clear impact of halogens on surface HO_x concentrations, with up to a 30 times increase at the surface when the halogen snow and recycling emissions are active. This increase is largest within the daytime surface layer, coinciding with the high levels of simulated chlorine atoms, and is shown in Figure 9b as a ratio of HO_x between the BASE and NOSURF runs. Modelled Cl atom concentration at noon is higher than the average concentration predicted during the campaign of 2.0×10^5 atoms cm^{-3} (Liao et al., 2014). We calculate values of 2.9×10^5 and 1.1×10^6 atoms cm^{-3} for 18 and 19 March at noon, respectively. Our higher values can partly be explained by the overestimation of modelled Cl_2 on day 2, as well as the higher Cl_2 levels observed during this period compared to the campaign average Cl_2 levels.

Figure 9c shows the calculated OH/HO_2 ratio at 1.5 m AGL in the NOSURF and BASE model runs. We find a significant shift in the OH/HO_2 ratio towards HO_2 in our BASE run following the addition of halogen emissions compared to the NOSURF run. This difference is largest during the day, within the lowest 40 m of the atmosphere, with up to an order of magnitude difference, as shown in Figure 9d. This shift towards HO_2 in the BASE run can be explained by two main reasons. Firstly, with the chlorine sources active in the BASE run, HO_2 formation via Cl-mediated VOC oxidation is greatly increased, skewing the ratio towards HO_2. This is in support of previous studies, which have suggested that HO_2 can be increased by the presence of chlorine, shifting the OH/HO_2 ratio significantly towards HO_2 (Piot & von Glasow, 2009; Rudolph et al., 1999; Thompson et al., 2015). Secondly, as the model was not constrained to any observations, the addition of halogen sources had a significant impact on the NO_x concentrations. Surface NO_x levels in the NOSURF run were several times greater than the BASE run, which greatly impacted OH formation. Thomas et al. (2012) showed that modelled surface concentrations of OH double with the inclusion of snowpack NO_x sources and bromine chemistry. This was mainly driven by the NO + HO_2 reaction under conditions where the halogen concentrations were significantly lower than those measured at Utqiaġvik during OASIS. In order to further understand HO_x cycling in our model, we analyse the major production and loss reactions of both OH and HO_2.

5.7.1 HO_x chemical budget

The main HO_x production and loss reactions at two heights (1.5 and 50.5 m) above the snow are shown in Figure 10. A clear chemical reactivity gradient is shown, with rates at 1.5 m approximately an order of magnitude greater than at 50.5 m, due to increased HO_x and Cl atom concentrations in the lower atmosphere. The principal OH production source in the model is the HO_2 recycling reaction with NO, at both the surface and above the boundary layer at 50.5 m AGL. Halogen-influenced OH production is clearly shown at 1.5 m, accounting for almost a quarter of surface OH production, with photolysis of HOBr (R6) contributing 14% and reactions involving chlorine comprising nearly 10%. This is a significant direct impact of snow-sourced halogens on the OH concentration. Snow emissions of other species, such as nitrous acid (HONO) and hydrogen peroxide (H_2O_2), could also be important sources of OH which may not be fully represented by our simulations due to missing snow emissions of these species in our model runs. At 50.5 m, modelled halogen concentrations are low with limited contribution to OH production at this height. Reaction between ozone and HO_2 is the second most important pathway for OH production at this height and is particularly important as it continues to convert HO_2 to OH for several hours after sunset. OH is lost via a multitude of reactions with organics, which can both recycle OH back into HO_2 and act as a source of CH_3O_2 and RO_2. Mainly, OH loss is dominated by the reaction with CO, accounting for approximately a quarter of OH loss at both heights, which is also an important source of HO_2.

At 1.5 m, the main HO_2 production reaction is the $CH_3O_2 + NO$ reaction (25%), followed by $CO + OH$ (16%). CH_3O_2 is formed following oxidation of VOCs and methane by OH and Cl, with the rate constant of $Cl + CH_4$ roughly an order of magnitude greater than $OH + CH_4$. Figure 11 shows the major production reactions of CH_3O_2 in our BASE run, with $Cl + CH_4$ responsible for almost two-thirds (64%) of surface CH_3O_2 production, whereas $OH + CH_4$ accounts for only 5%. At 50.5 m above the surface, production via $Cl + CH_4$ is negligible due to the low abundance of Cl atoms. Therefore, we can determine that snow emissions of chlorine drive the increase of surface HO_2 levels via CH_3O_2 formation. Consequently, this reaction cycle can also accelerate bromine recycling and ozone depletion, via (R5), linking together the chlorine and bromine chemical cycles. This effect is seen at 1.5 m, with BrO constituting 8% of HO_2 loss, with minimal contribution at 50.5 m.

In summary, it can be clearly seen that halogen emissions from snow make a significant contribution to HO_x production and loss reactions close to the surface. Chlorine and bromine chemical cycles are linked via peroxy radical formation, enhancing HO_x chemistry within the boundary layer, which can significantly impact VOC reactivity and lifetimes.

5.7.2 VOC chemical lifetimes

VOCs were measured during the campaign and the impact of Cl and Br atoms on VOC concentrations are discussed in detail in Hornbrook et al. (2016). The influence of chlorine chemistry on VOCs was determined during the campaign by recording the ratio of isobutane to n-butane (iC_4/C_4), as both alkanes react at similar rates with OH, but n-butane reacts approximately 1.5 times faster with Cl. iC_4/C_4 rose over the course of the campaign, indicating increased Cl-atom processing (and Cl_2 production) with increased availability of sunlight as spring progressed. Table 4 shows the simulated OH and Cl atoms concentrations at 1.5 m and 50.5 m AGL used to calculate the chemical lifetimes (τ) of several VOCs presented in Table 5. For computational efficiency, some species within the RACM2 mechanism with similar reactivities are lumped together and treated as one species, such as propane and other similar organic compounds (HC3), as well as for pentane (HC5) and octane (HC8). At the surface, Cl atoms are abundant and rapidly oxidize VOCs, typically on the order of several hours, compared to OH which is generally on the order of days. As previously shown, surface OH concentration increases following the addition of halogen emissions, resulting in a reduction of VOC lifetimes by roughly 43% compared to the NOSURF run. This is a significant increase in the reactivity and processing of VOCs via OH due to the presence of halogens. At 50.5 m above the surface, this difference is minimal as levels of halogen radicals are very low, demonstrating the impact of chlorine chemistry close to the ground. We also see a clear gradient in chemical lifetimes with height and would expect longer lived VOCs above the boundary layer to act as a reservoir and replenish surface VOC concentrations by downward transport.

Indeed, as shown in Hornbrook et al. (2016), the VOCs sampled indicated more important halogen influence on atmospheric chemistry between the early hours of 18 March and 19 March. These VOC observations are likely a mix of local chemistry that is represented within our 1D model and chemistry that occurred while air masses resided over sea ice prior to sampling. Hornbrook et al. (2016) used ethyne levels to show there was a fairly consistent, but moderately low, Br-atom influence atmospheric chemistry on 18 March. At the same time, measured acetaldehyde, propanal, and butanal decreased by approximately 50%, 75% and 90% respectively (see Figure 14 in Hornbrook et al. (2016)). As well, the butanal observations indicated a gradient between the lowest sampling height, 0.6 m, and the other two sampling heights at 1.5 and 5.4 m, in which the mixing ratio nearest the snow surface reached levels as low as half that at the higher sampling inlets, consistent with Cl-atom chemistry near the surface. Overall, our results show that mea-

surements above the Arctic snow surface can be highly influenced by halogen chemistry directly or indirectly via increases in HO_x concentration, resulting in a highly reactive surface layer.

6 Conclusions

In this study, we examined the role of Arctic halogen emissions from snow on boundary layer oxidation processes using an updated version of the PACT-1D model. Snow emissions of Cl_2 and Br_2 were added to the model, including primary production from surface snow and heterogeneous recycling on aerosols and snow. We compared the model against observations from the 2009 OASIS campaign at Utqiaġvik, Alaska, when high atmospheric Cl_2 levels were observed ($18-19$ March). The modelled halogen concentrations showed excellent agreement with the observations upon the addition of halogen emissions. The main conclusions of our study can be summarised as follows:

- Surface Arctic halogen observations are reproduced by the model when including the combined effects of halogen emissions from snow, vertical mixing and atmospheric chemistry. Primary emissions of Cl_2 from snow, parameterized using solar irradiance and measured surface ozone concentration, can describe surface observations of Arctic Cl_2. Modelled Br_2 levels are in good agreement with observations when using a combination of both primary emissions from snow and heterogeneous surface recycling of $BrONO_2$ and HOBr. Sensitivity analyses showed that increased heterogeneous recycling of halogens on aerosols could not explain surface observations and only provided a minor source of reactive halogens in our model simulations (AERO simulation).
- Boundary layer dynamics, vertical mixing, chemistry and emissions all strongly impact halogen vertical distribution. During the day, Cl_2 is confined to within the lowest 15 m of the atmosphere on both days of the simulation period. Stable conditions during this period resulted in a shallow surface layer, hindering vertical mixing and impacting surface concentrations. In particular, changes in the model vertical mixing and boundary layer dynamics result in a reduction of up to 60 pptv of Cl_2 at 1.5 m during the day (PBLH simulation).
- HO_x radical concentration is increased by up to a factor of 30 with the inclusion of halogen emissions in the model. The increase in OH was primarily driven by elevated HOBr levels and its subsequent photolysis (R6). A significant contributor of HO_2 production is the CH_3O_2 radical formed via the Cl + CH_4 reaction (R4). This also caused a decrease in the modelled OH/HO_2 ratio which is attributable to chlorine chemistry.
- Increased HO_x radicals and a high Cl-atom concentration near the surface significantly increases chemical reactivity within a shallow layer near the surface. Modelled VOC lifetimes, with respect to OH, are reduced by approximately 43% due to the presence of halogens (BASE run). Cl atoms concentrated near the surface rapidly react with VOCs, but this reactivity becomes much weaker with height and negligible over 15 m above the surface.

Additional modelling studies at different snow covered regions are desirable to further test the conclusions and model parameterizations in this study under different meteorological conditions. This, together with added field measurements of vertically resolved halogens, can help improve our understanding of snow-produced halogens and their impact on atmospheric chemistry. Future work will focus on the development of these parameterizations to include halogen emissions from snow in 3D numerical models. Due to resolution constraints of 3D models, implementation and testing of halogen emissions from snow remains a challenge. This could potentially be addressed by implementing a sub-grid scale parameterization to describe these processes in regional and global chem-

ical transport models. Ultimately, the consideration of halogen emissions from snow in models is necessary to accurately simulate polar boundary layer oxidation processes.

Acknowledgments

The code for the model and input files are all publicly available on Zenodo as Ahmed et al. (2021) `https://doi.org/10.5281/zenodo.5654589`. The model outputs for the BASE run can also be found on Zenodo at `https://doi.org/10.5281/zenodo.5654628`. The data for this campaign are publicly available through the NSF Arctic Data Center at `https://arcticdata.io/`. This work was supported by the Ecole Doctorale Sciences de la Terre, de l'Environnement et des Planètes (ED105) of Université Grenoble Alpes. We also acknowledge support by the CNRS INSU LEFE-CHAT program under the grant Brom-Arc. This material is based upon work supported by the National Center for Atmospheric Research, which is a major facility sponsored by the National Science Foundation under Cooperative Agreement No. 1852977. We acknowledge support for Detlev Helmig and Patrick Boylan from the NSF grant 0902165. We acknowledge the additional support to NCAR under the NSF grant 0806437. We also acknowledge support under the NSF grant 0732556. We thank the entire OASIS team involved in the campaign and the collection of data with special thanks to: Jin Liao, Andrew Weinheimer, Jim Smith, Roy Mauldin, James Walega, Petter Weibring and Dirk Richter. We also thank colleagues Aurélien Dommergue, Didier Voisin, Anna Jones and Thorsten Bartels-Rausch for meaningful scientific discussions.

References

Abbatt, J. P. D., Thomas, J. L., Abrahamsson, K., Boxe, C., Granfors, A., Jones, A. E., ... Yang, X. (2012). Halogen activation via interactions with environmental ice and snow in the polar lower troposphere and other regions. *Atmospheric Chemistry and Physics*, *12*(14), 6237–6271. doi: 10.5194/acp-12-6237-2012

Aguzzi, A., & J. Rossi, M. (1999). The kinetics of the heterogeneous reaction of $BrONO_2$ with solid alkali halides at ambient temperature. A comparison with the interaction of $ClONO_2$ on NaCl and KBr. *Physical Chemistry Chemical Physics*, *1*, 4337–4346. doi: 10.1039/A904611I

Ahmed, S., Thomas, J. L., Tuite, K., & Stutz, J. (2021). *PACT-1D model version including polar chlorine and bromine emission mechanisms.* Zenodo. Retrieved from `https://doi.org/10.5281/zenodo.5654589` doi: 10.5281/zenodo.5654589

Ammann, M., Cox, R. A., Crowley, J. N., Jenkin, M. E., Mellouki, A., Rossi, M. J., ... Wallington, T. J. (2013). Evaluated kinetic and photochemical data for atmospheric chemistry: Volume VI – heterogeneous reactions with liquid substrates. *Atmospheric Chemistry and Physics*, *13*(16), 8045–8228. doi: 10.5194/acp-13-8045-2013

Anderson, P. S., & Neff, W. D. (2008). Boundary layer physics over snow and ice. *Atmospheric Chemistry and Physics*, *8*(13), 3563–3582. doi: 10.5194/acp-8-3563-2008

Apel, E. C. (2009). *VOC measurements during OASIS Barrow field intensive Spring 2009.* `https://arcticdata.io/catalog/view/doi:10.5065/D6DB7ZXF`. Arctic Data Center. (Accessed on 08/24/2021) doi: 10.5065/D6DB7ZXF

Atkinson, R., Baulch, D. L., Cox, R. A., Crowley, J. N., Hampson, R. F., Hynes, R. G., ... IUPAC Subcommittee (2006). Evaluated kinetic and photochemical data for atmospheric chemistry: Volume II – gas phase reactions of organic species. *Atmospheric Chemistry and Physics*, *6*(11), 3625–4055. doi: 10.5194/acp-6-3625-2006

Barret, M., Domine, F., Houdier, S., Gallet, J.-C., Weibring, P., Walega, J., ...

Richter, D. (2011). Formaldehyde in the Alaskan Arctic snowpack: Partitioning and physical processes involved in air-snow exchanges. *Journal of Geophysical Research: Atmospheres*, *116*(D14). doi: 10.1029/2011JD016038

Barrie, L. A., Bottenheim, J. W., Schnell, R. C., Crutzen, P. J., & Rasmussen, R. A. (1988). Ozone destruction and photochemical reactions at polar sunrise in the lower Arctic atmosphere. *Nature*, *334*(6178), 138–141. doi: 10.1038/334138a0

Bartels-Rausch, T., Jacobi, H.-W., Kahan, T. F., Thomas, J. L., Thomson, E. S., Abbatt, J. P. D., ... Sodeau, J. R. (2014). A review of air–ice chemical and physical interactions (AICI): liquids, quasi-liquids, and solids in snow. *Atmospheric Chemistry and Physics*, *14*(3), 1587–1633. doi: 10.5194/acp-14-1587-2014

Boylan, P., Helmig, D., Staebler, R., Turnipseed, A., Fairall, C., & Neff, W. (2014). Boundary layer dynamics during the Ocean-Atmosphere-Sea-Ice-Snow (OASIS) 2009 experiment at Barrow, AK. *Journal of Geophysical Research: Atmospheres*, *119*(5), 2261–2278. doi: 10.1002/2013JD020299

Brioude, J., Arnold, D., Stohl, A., Cassiani, M., Morton, D., Seibert, P., ... Wotawa, G. (2013). The Lagrangian particle dispersion model FLEXPART-WRF version 3.1. *Geoscientific Model Development*, *6*(6), 1889–1904. doi: 10.5194/gmd-6-1889-2013

Buchholz, R. R., Emmons, L. K., Tilmes, S., & The CESM2 Development Team. (2019). *CESM2.1/CAM-chem Instantaneous Output for Boundary Conditions.* UCAR/NCAR - Atmospheric Chemistry Observations and Modeling Laboratory. Subset used Lat: 50 to 90, Lon: 120 to 250, 18 March 2009 - 18 March 2009, Accessed: 09/07/2020. doi: 10.5065/NMP7-EP60

Burkholder, J. B., Sander, S. P., Abbatt, J., Barker, J. R., Cappa, C., Crounse, J. D., ... Wine, P. H. (2019). *Chemical Kinetics and Photochemical Data for Use in Atmospheric Studies, Evaluation No. 19,.* JPL Publication 19-5, Jet Propulsion Laboratory, Pasadena. Retrieved from `http://jpldataeval.jpl.nasa.gov/`

Calvert, J. G., Orlando, J. J., Stockwell, W. R., & Wallington, T. J. (2015). *The mechanisms of reactions influencing atmospheric ozone.* Oxford University Press.

Cantrell, C. A. (2009). *HO_2 and RO_2 measurements during OASIS Barrow field intensive Spring 2009.* `https://arcticdata.io/catalog/view/doi:10.5065/D6GH9G2J`. Arctic Data Center. (Accessed on 08/24/2021) doi: 10.5065/D6GH9G2J

Cao, L., Platt, U., & Gutheil, E. (2016). Role of the boundary layer in the occurrence and termination of the tropospheric ozone depletion events in polar spring. *Atmospheric Environment*, *132*, 98–110. doi: 10.1016/j.atmosenv.2016.02.034

Custard, K. D., Pratt, K. A., Wang, S., & Shepson, P. B. (2016). Constraints on Arctic Atmospheric Chlorine Production through Measurements and Simulations of Cl_2 and ClO. *Environmental Science & Technology*, *50*(22), 12394–12400. doi: 10.1021/acs.est.6b03909

Custard, K. D., Raso, A. R. W., Shepson, P. B., Staebler, R. M., & Pratt, K. A. (2017). Production and Release of Molecular Bromine and Chlorine from the Arctic Coastal Snowpack. *ACS Earth and Space Chemistry*, *1*(3), 142–151. doi: 10.1021/acsearthspacechem.7b00014

Custard, K. D., Thompson, C. R., Pratt, K. A., Shepson, P. B., Liao, J., Huey, L. G., ... Montzka, D. D. (2015). The NO_x dependence of bromine chemistry in the Arctic atmospheric boundary layer. *Atmospheric Chemistry and Physics*, *15*(18), 10799–10809. doi: 10.5194/acp-15-10799-2015

Deiber, G., George, C., Le Calvé, S., Schweitzer, F., & Mirabel, P. (2004). Uptake study of $ClONO_2$ and $BrONO_2$ by Halide containing droplets. *Atmospheric Chemistry and Physics*, *4*(5), 1291–1299. doi: 10.5194/acp-4-1291-2004

Domine, F., Albert, M., Huthwelker, T., Jacobi, H.-W., Kokhanovsky, A. A., Lehning, M., ... Simpson, W. R. (2008). Snow physics as relevant to snow photochemistry. *Atmospheric Chemistry and Physics*, *8*(2), 171–208. doi: 10.5194/acp-8-171-2008

Domine, F., Bock, J., Voisin, D., & Donaldson, D. J. (2013). Can We Model Snow Photochemistry? Problems with the Current Approaches. *The Journal of Physical Chemistry A*, *117*(23), 4733–4749. doi: 10.1021/jp3123314

Durre, I., Vose, R. S., & Wuertz, D. B. (2006). Overview of the Integrated Global Radiosonde Archive. *Journal of Climate*, *19*(1), 53–68. doi: 10.1175/JCLI3594.1

Emmons, L. K., Schwantes, R. H., Orlando, J. J., Tyndall, G., Kinnison, D., Lamarque, J.-F., ... Pétron, G. (2020). The Chemistry Mechanism in the Community Earth System Model Version 2 (CESM2). *Journal of Advances in Modeling Earth Systems*, *12*(4), e2019MS001882. doi: 10.1029/2019MS001882

Falk, S., & Sinnhuber, B.-M. (2018). Polar boundary layer bromine explosion and ozone depletion events in the chemistry–climate model EMAC v2.52: implementation and evaluation of AirSnow algorithm. *Geoscientific Model Development*, *11*(3), 1115–1131. doi: 10.5194/gmd-11-1115-2018

Fernandez, R. P., Carmona-Balea, A., Cuevas, C. A., Barrera, J. A., Kinnison, D. E., Lamarque, J.-F., ... Saiz-Lopez, A. (2019). Modeling the Sources and Chemistry of Polar Tropospheric Halogens (Cl, Br, and I) Using the CAM-Chem Global Chemistry-Climate Model. *Journal of Advances in Modeling Earth Systems*, *11*(7), 2259-2289. doi: 10.1029/2019MS001655

Finlayson-Pitts, B. J., Ezell, M. J., & Pitts, J. N. (1989). Formation of chemically active chlorine compounds by reactions of atmospheric NaCl particles with gaseous N_2O_5 and $ClONO_2$. *Nature*, *337*(6204), 241–244. doi: 10.1038/337241a0

Frey, M. M., Roscoe, H. K., Kukui, A., Savarino, J., France, J. L., King, M. D., ... Preunkert, S. (2015). Atmospheric nitrogen oxides (NO and NO_2) at Dome C, East Antarctica, during the OPALE campaign. *Atmospheric Chemistry and Physics*, *15*(14), 7859–7875. doi: 10.5194/acp-15-7859-2015

Fried, A. (2009). *Formaldehyde measurements during OASIS Barrow field intensive Spring 2009.* `https://arcticdata.io/catalog/view/doi:10.5065/D63B5X7H`. Arctic Data Center. (Accessed on 08/24/2021) doi: 10.5065/D63B5X7H

Goliff, W. S., Stockwell, W. R., & Lawson, C. V. (2013). The regional atmospheric chemistry mechanism, version 2. *Atmospheric Environment*, *68*, 174–185. doi: 10.1016/j.atmosenv.2012.11.038

Grannas, A. M., Jones, A. E., Dibb, J., Ammann, M., Anastasio, C., Beine, H. J., ... Zhu, T. (2007). An overview of snow photochemistry: evidence, mechanisms and impacts. *Atmospheric Chemistry and Physics*, *7*(16), 4329–4373. doi: 10.5194/acp-7-4329-2007

Guenther, A. B. (2009). *Meteorology measurements during OASIS Barrow field intensive Spring 2009.* `https://arcticdata.io/catalog/view/doi:10.5065/D62J6902`. Arctic Data Center. (Accessed on 08/24/2021) doi: 10.5065/D62J6902

Hall, D. K., & Riggs, G. A. (2021). *MODIS/Terra Snow Cover Daily L3 Global 0.05Deg CMG, Version 61.* Subset used: 19 March 2009. Boulder, Colorado USA. NASA National Snow and Ice Data Center Distributed Active Archive Center. (Accessed January 30 2021) doi: 10.5067/MODIS/MOD10C1.061

Hall, S. R. (2009). *Actinic Flux measurements during OASIS Barrow field intensive Spring 2009.* `https://arcticdata.io/catalog/view/doi:10.5065/D6GB2260`. Arctic Data Center. (Accessed on 08/24/2021) doi: 10.5065/D6GB2260

Helmig, D., Boylan, P., Johnson, B., Oltmans, S., Fairall, C., Staebler, R., ... Shep-

son, P. B. (2012). Ozone dynamics and snow-atmosphere exchanges during ozone depletion events at Barrow, Alaska. *Journal of Geophysical Research: Atmospheres*, *117*, D20303. doi: 10.1029/2012JD017531

Herrmann, M., Cao, L., Sihler, H., Platt, U., & Gutheil, E. (2019). On the contribution of chemical oscillations to ozone depletion events in the polar spring. *Atmospheric Chemistry and Physics*, *19*(15), 10161–10190. doi: 10.5194/acp-19-10161-2019

Herrmann, M., Sihler, H., Frieß, U., Wagner, T., Platt, U., & Gutheil, E. (2021). Time-dependent 3D simulations of tropospheric ozone depletion events in the Arctic spring using the Weather Research and Forecasting model coupled with Chemistry (WRF-Chem). *Atmospheric Chemistry and Physics*, *21*(10), 7611–7638. doi: 10.5194/acp-21-7611-2021

Honrath, R. E., Lu, Y., Peterson, M. C., Dibb, J. E., Arsenault, M. A., Cullen, N. J., & Steffen, K. (2002). Vertical fluxes of NO_x, HONO, and HNO_3 above the snowpack at Summit, Greenland. *Atmospheric Environment*, *36*(15), 2629–2640. doi: 10.1016/S1352-2310(02)00132-2

Honrath, R. E., Peterson, M. C., Guo, S., Dibb, J. E., Shepson, P. B., & Campbell, B. (1999). Evidence of NO_x production within or upon ice particles in the Greenland snowpack. *Geophysical Research Letters*, *26*(6), 695-698. doi: 10.1029/1999GL900077

Hornbrook, R. S., Crawford, J. H., Edwards, G. D., Goyea, O., Mauldin III, R. L., Olson, J. S., & Cantrell, C. A. (2011). Measurements of tropospheric HO_2 and RO_2 by oxygen dilution modulation and chemical ionization mass spectrometry. *Atmospheric Measurement Techniques*, *4*(4), 735–756. doi: 10.5194/amt-4-735-2011

Hornbrook, R. S., Hills, A. J., Riemer, D. D., Abdelhamid, A., Flocke, F. M., Hall, S. R., ... Apel, E. C. (2016). Arctic springtime observations of volatile organic compounds during the OASIS-2009 campaign. *Journal of Geophysical Research: Atmospheres*, *121*(16), 9789–9813. doi: 10.1002/2015JD024360

Hu, J. H., Shi, Q., Davidovits, P., Worsnop, D. R., Zahniser, M. S., & Kolb, C. E. (1995). Reactive Uptake of $Cl_{2(g)}$ and $Br_{2(g)}$ by Aqueous Surfaces as a Function of Br^- and I^- Ion Concentration: The Effect of Chemical Reaction at the Interface. *The Journal of Physical Chemistry*, *99*(21), 8768–8776. doi: 10.1021/j100021a050

IUPAC. (2009). *IUPAC Task Group on Atmospheric Chemical Kinetic Data Evaluation.* Retrieved from `https://iupac-aeris.ipsl.fr/`

Kahl, J. D. (1990). Characteristics of the low-level temperature inversion along the Alaskan Arctic coast. *International Journal of Climatology*, *10*(5), 537–548. doi: 10.1002/joc.3370100509

Knipping, E. M., Lakin, M. J., Foster, K. L., Jungwirth, P., Tobias, D. J., Gerber, R. B., ... Finlayson-Pitts, B. J. (2000). Experiments and Simulations of Ion-Enhanced Interfacial Chemistry on Aqueous NaCl Aerosols. *Science*, *288*(5464), 301–306. doi: 10.1126/science.288.5464.301

Laskin, A., Wang, H., Robertson, W. H., Cowin, J. P., Ezell, M. J., & Finlayson-Pitts, B. J. (2006). A New Approach to Determining Gas-Particle Reaction Probabilities and Application to the Heterogeneous Reaction of Deliquesced Sodium Chloride Particles with Gas-Phase Hydroxyl Radicals. *The Journal of Physical Chemistry A*, *110*(36), 10619–10627. doi: 10.1021/jp063263+

Lehrer, E., Hönninger, G., & Platt, U. (2004). A one dimensional model study of the mechanism of halogen liberation and vertical transport in the polar troposphere. *Atmospheric Chemistry and Physics*, *4*, 2427-2440. doi: 10.5194/acp-4-2427-2004

Liao, J., Huey, L. G., Liu, Z., Tanner, D. J., Cantrell, C. A., Orlando, J. J., ... Nowak, J. B. (2014). High levels of molecular chlorine in the Arctic atmosphere. *Nature Geoscience*, *7*(2), 91–94. doi: 10.1038/ngeo2046

Liao, J., Huey, L. G., Tanner, D. J., Flocke, F. M., Orlando, J. J., Neuman, J. A., ... Stephens, C. R. (2012). Observations of inorganic bromine (HOBr, BrO, and Br_2) speciation at Barrow, Alaska, in spring 2009. *Journal of Geophysical Research: Atmospheres*, *117*, D00R16. doi: 10.1029/2011JD016641

Liao, J., Sihler, H., Huey, L. G., Neuman, J. A., Tanner, D. J., Friess, U., ... Ullmann, K. (2011). A comparison of Arctic BrO measurements by chemical ionization mass spectrometry and long path-differential optical absorption spectroscopy. *Journal of Geophysical Research: Atmospheres*, *116*, D00R02. doi: 10.1029/2010JD014788

Liu, X., Qu, H., Huey, L. G., Wang, Y., Sjostedt, S., Zeng, L., ... Zhang, Y. (2017). High Levels of Daytime Molecular Chlorine and Nitryl Chloride at a Rural Site on the North China Plain. *Environmental Science & Technology*, *51*(17), 9588–9595. doi: 10.1021/acs.est.7b03039

Madronich, S., & Flocke, S. (1999). The Role of Solar Radiation in Atmospheric Chemistry. In *The Handbook of Environmental Photochemistry* (pp. 1–26). Berlin, Heidelberg: Springer Berlin Heidelberg. doi: 10.1007/978-3-540-69044-3_1

Marelle, L., Raut, J.-C., Law, K. S., Berg, L. K., Fast, J. D., Easter, R. C., ... Thomas, J. L. (2017). Improvements to the WRF-Chem 3.5.1 model for quasi-hemispheric simulations of aerosols and ozone in the Arctic. *Geoscientific Model Development*, *10*(10), 3661–3677. doi: 10.5194/gmd-10-3661-2017

Marelle, L., Thomas, J. L., Ahmed, S., Tuite, K., Stutz, J., Dommergue, A., ... Baladima, F. (2021). Implementation and impacts of surface and blowing snow sources of Arctic bromine activation within WRF-Chem 4.1.1. *Journal of Advances in Modeling Earth Systems*, *13*, e2020MS002391. doi: 10.1029/2020MS002391

Mauldin III, R. L., Frost, G. J., Chen, G., Tanner, D. J., Prevot, A. S. H., Davis, D. D., & Eisele, F. L. (1998). OH measurements during the First Aerosol Characterization Experiment (ACE 1): Observations and model comparisons. *Journal of Geophysical Research: Atmospheres*, *103*(D13), 16713-16729. doi: 10.1029/98JD00882

McNamara, S. M., Garner, N. M., Wang, S., Raso, A. R. W., Thanekar, S., Barget, A. J., ... Pratt, K. A. (2020). Bromine Chloride in the Coastal Arctic: Diel Patterns and Production Mechanisms. *ACS Earth and Space Chemistry*, *4*(4), 620–630. doi: 10.1021/acsearthspacechem.0c00021

McNamara, S. M., Raso, A. R. W., Wang, S., Thanekar, S., Boone, E. J., Kolesar, K. R., ... Pratt, K. A. (2019). Springtime Nitrogen Oxide-Influenced Chlorine Chemistry in the Coastal Arctic. *Environmental Science & Technology*, *53*(14), 8057–8067. doi: 10.1021/acs.est.9b01797

McNeill, V. F., Grannas, A. M., Abbatt, J. P. D., Ammann, M., Ariya, P., Bartels-Rausch, T., ... Voisin, D. (2012). Organics in environmental ices: sources, chemistry, and impacts. *Atmospheric Chemistry and Physics*, *12*(20), 9653–9678. doi: 10.5194/acp-12-9653-2012

Melsheimer, C., & Spreen, G. (2020). *AMSR-E ASI sea ice concentration data, Arctic, version 5.4 (NetCDF) (June 2002 - September 2011)*. PANGAEA. doi: 10.1594/PANGAEA.919777

Neff, W., Helmig, D., Grachev, A., & Davis, D. (2008). A study of boundary layer behavior associated with high NO concentrations at the South Pole using a minisodar, tethered balloon, and sonic anemometer. *Atmospheric Environment*, *42*(12), 2762-2779. doi: 10.1016/j.atmosenv.2007.01.033

Oltmans, S. J., Johnson, B. J., & Harris, J. M. (2012). Springtime boundary layer ozone depletion at Barrow, Alaska: Meteorological influence, year-to-year variation, and long-term change. *Journal of Geophysical Research: Atmospheres*, *117*, D00R18. doi: 10.1029/2011JD016889

Parrish, D. D., Holloway, J. S., & Fehsenfeld, F. C. (1994). Routine, Continuous

Measurement of Carbon Monoxide with Parts per Billion Precision. *Environmental Science & Technology*, *28*(9), 1615–1618. doi: 10.1021/es00058a013

Piot, M., & von Glasow, R. (2008). The potential importance of frost flowers, recycling on snow, and open leads for ozone depletion events. *Atmospheric Chemistry and Physics*, *8*(9), 2437–2467. doi: 10.5194/acp-8-2437-2008

Piot, M., & von Glasow, R. (2009). Modelling the multiphase near-surface chemistry related to ozone depletions in polar spring. *Journal of Atmospheric Chemistry*, *64*(2), 77–105. doi: 10.1007/s10874-010-9170-1

Platt, U., & Hönninger, G. (2003). The role of halogen species in the troposphere. *Chemosphere*, *52*(2), 325–338. doi: 10.1016/S0045-6535(03)00216-9

Pollard, R. T., Rhines, P. B., & Thompson, R. O. R. Y. (1973). The deepening of the wind-Mixed layer. *Geophysical Fluid Dynamics*, *4*(4), 381–404. doi: 10.1080/03091927208236105

Pratt, K. A., Custard, K. D., Shepson, P. B., Douglas, T. A., Pöhler, D., General, S., ... Stirm, B. H. (2013). Photochemical production of molecular bromine in Arctic surface snowpacks. *Nature Geoscience*, *6*(5), 351–356. doi: 10.1038/ngeo1779

Pratte, P., & Rossi, M. J. (2006). The heterogeneous kinetics of HOBr and HOCl on acidified sea salt and model aerosol at 40–90% relative humidity and ambient temperature. *Physical Chemistry Chemical Physics*, *8*, 3988–4001. doi: 10.1039/B604321F

Rudolph, J., Ru Fu, B., Thompson, A., Anlauf, K., & Bottenheim, J. (1999). Halogen atom concentrations in the Arctic Troposphere derived from hydrocarbon measurements: Impact on the budget of formaldehyde. *Geophysical Research Letters*, *26*(19), 2941-2944. doi: 10.1029/1999GL010869

Sandu, A., & Sander, R. (2006). Technical note: Simulating chemical systems in Fortran90 and Matlab with the Kinetic PreProcessor KPP-2.1. *Atmospheric Chemistry and Physics*, *6*(1), 187–195. doi: 10.5194/acp-6-187-2006

Seisel, S., Flückiger, B., & Rossi, M. J. (1998). The heterogeneous reaction of N_2O_5 with HBr on Ice comparison with N_2O_5+HCl. *Berichte der Bunsengesellschaft für physikalische Chemie*, *102*(6), 811–820. doi: 10.1002/bbpc.19981020604

Shetter, R. E., & Müller, M. (1999). Photolysis frequency measurements using actinic flux spectroradiometry during the PEM-Tropics mission: Instrumentation description and some results. *Journal of Geophysical Research: Atmospheres*, *104*(D5), 5647–5661. doi: 10.1029/98JD01381

Simpson, W. R., Brown, S. S., Saiz-Lopez, A., Thornton, J. A., & von Glasow, R. (2015). Tropospheric Halogen Chemistry: Sources, Cycling, and Impacts. *Chemical Reviews*, *115*(10), 4035–4062. doi: 10.1021/cr5006638

Simpson, W. R., von Glasow, R., Riedel, K., Anderson, P., Ariya, P., Bottenheim, J., ... Wolff, E. (2007). Halogens and their role in polar boundary-layer ozone depletion. *Atmospheric Chemistry and Physics*, *7*(16), 4375–4418. doi: 10.5194/acp-7-4375-2007

Skamarock, W. C., Klemp, J. B., Dudhia, J., Gill, D. O., Liu, Z., Berner, J., ... Huang, X.-Y. (2019). *A Description of the Advanced Research WRF Version 4.* (Tech. Rep.). Note NCAR/TN-556+STR, 145 pp. doi: 10.5065/1dfh-6p97

Smith, J., Sjostedt, S., Abbatt, J., & Wiedensohler, A. (2009). *Aerosol measurements during OASIS Barrow field intensive Spring 2009.* `https://arcticdata.io/catalog/view/doi:10.5065/D6P8491K`. Arctic Data Center. (Accessed on 08/24/2021) doi: 10.5065/D6P8491K

Spreen, G., Kaleschke, L., & Heygster, G. (2008). Sea ice remote sensing using AMSR-E 89-GHz channels. *Journal of Geophysical Research: Oceans*, *113*(C2). doi: 10.1029/2005JC003384

Steffen, A., Bottenheim, J., Cole, A., Douglas, T. A., Ebinghaus, R., Friess, U., ... Staebler, R. (2013). Atmospheric mercury over sea ice during the OASIS-2009 campaign. *Atmospheric Chemistry and Physics*, *13*(14), 7007–7021. doi:

10.5194/acp-13-7007-2013

Steffen, A., Douglas, T., Amyot, M., Ariya, P., Aspmo, K., Berg, T., ... Temme, C. (2008). A synthesis of atmospheric mercury depletion event chemistry in the atmosphere and snow. *Atmospheric Chemistry and Physics*, *8*(6), 1445–1482. doi: 10.5194/acp-8-1445-2008

Tanner, D. J., Jefferson, A., & Eisele, F. L. (1997). Selected ion chemical ionization mass spectrometric measurement of OH. *Journal of Geophysical Research: Atmospheres*, *102*(D5), 6415-6425. doi: 10.1029/96JD03919

Thomas, J. L., Dibb, J. E., Huey, L. G., Liao, J., Tanner, D., Lefer, B., ... Stutz, J. (2012). Modeling chemistry in and above snow at Summit, Greenland – Part 2: Impact of snowpack chemistry on the oxidation capacity of the boundary layer. *Atmospheric Chemistry and Physics*, *12*(14), 6537–6554. doi: 10.5194/acp-12-6537-2012

Thomas, J. L., Stutz, J., Lefer, B., Huey, L. G., Toyota, K., Dibb, J. E., & von Glasow, R. (2011). Modeling chemistry in and above snow at Summit, Greenland – Part 1: Model description and results. *Atmospheric Chemistry and Physics*, *11*(10), 4899–4914. doi: 10.5194/acp-11-4899-2011

Thompson, C. R., Shepson, P. B., Liao, J., Huey, L. G., Apel, E. C., Cantrell, C. A., ... Weinheimer, A. (2015). Interactions of bromine, chlorine, and iodine photochemistry during ozone depletions in Barrow, Alaska. *Atmospheric Chemistry and Physics*, *15*(16), 9651–9679. doi: 10.5194/acp-15-9651-2015

Toyota, K., McConnell, J. C., Lupu, A., Neary, L., McLinden, C. A., Richter, A., ... Sioris, C. E. (2011). Analysis of reactive bromine production and ozone depletion in the Arctic boundary layer using 3-D simulations with GEM-AQ: inference from synoptic-scale patterns. *Atmospheric Chemistry and Physics*, *11*(8), 3949–3979. doi: 10.5194/acp-11-3949-2011

Toyota, K., McConnell, J. C., Staebler, R. M., & Dastoor, A. P. (2014). Air–snowpack exchange of bromine, ozone and mercury in the springtime Arctic simulated by the 1-D model PHANTAS – Part 1: In-snow bromine activation and its impact on ozone. *Atmospheric Chemistry and Physics*, *14*(8), 4101–4133. doi: 10.5194/acp-14-4101-2014

Tuite, K., Thomas, J. L., Veres, P. R., Roberts, J. M., Stevens, P. S., Griffith, S. M., ... Stutz, J. (2021). Quantifying nitrous acid formation mechanisms using measured vertical profiles during the CalNex 2010 campaign and 1D column modeling. *Journal of Geophysical Research: Atmospheres*, *126*, e2021JD034689. doi: 10.1029/2021JD034689

Villena, G., Wiesen, P., Cantrell, C. A., Flocke, F., Fried, A., Hall, S. R., ... Kleffmann, J. (2011). Nitrous acid (HONO) during polar spring in Barrow, Alaska: A net source of OH radicals? *Journal of Geophysical Research: Atmospheres*, *116*, D00R07. doi: 10.1029/2011JD016643

Wang, S., McNamara, S. M., Kolesar, K. R., May, N. W., Fuentes, J. D., Cook, R. D., ... Pratt, K. A. (2020). Urban Snowpack $ClNO_2$ Production and Fate: A One-Dimensional Modeling Study. *ACS Earth and Space Chemistry*, *4*(7), 1140–1148. doi: 10.1021/acsearthspacechem.0c00116

Wang, S., McNamara, S. M., Moore, C. W., Obrist, D., Steffen, A., Shepson, P. B., ... Pratt, K. A. (2019). Direct detection of atmospheric atomic bromine leading to mercury and ozone depletion. *Proceedings of the National Academy of Sciences*, *116*(29), 14479–14484. doi: 10.1073/pnas.1900613116

Wang, S., & Pratt, K. A. (2017). Molecular Halogens Above the Arctic Snowpack: Emissions, Diurnal Variations, and Recycling Mechanisms. *Journal of Geophysical Research: Atmospheres*, *122*(21), 11,991–12,007. doi: 10.1002/2017JD027175

Weibring, P., Richter, D., Walega, J. G., & Fried, A. (2007). First demonstration of a high performance difference frequency spectrometer on airborne platforms. *Optics Express*, *15*(21), 13476–13495. doi: 10.1364/OE.15.013476

Weibring, P., Richter, D., Walega, J. G., Rippe, L., & Fried, A. (2010). Difference frequency generation spectrometer for simultaneous multispecies detection. *Optics Express*, *18*(26), 27670–27681. doi: 10.1364/OE.18.027670

Weinheimer, A. J. (2009). *Ozone, NO_x, and NO_y measurements during OASIS Barrow field intensive Spring 2009.* `https://arcticdata.io/catalog/view/doi:10.5065/D6RJ4GK6`. Arctic Data Center. (Accessed on 08/24/2021) doi: 10.5065/D6RJ4GK6

Weinheimer, A. J., Montzka, D. D., Campos, T. L., Walega, J. G., Ridley, B. A., Donnelly, S. G., ... Newman, P. A. (1998). Comparison between DC-8 and ER-2 species measurements in the tropical middle troposphere: NO, NO_y, O_3, CO_2, CH_4, and N_2O. *Journal of Geophysical Research: Atmospheres*, *103*(D17), 22087-22096. doi: 10.1029/98JD01421

Woo, K. S., Chen, D. R., Pui, D. Y. H., & McMurry, P. H. (2001). Measurement of Atlanta Aerosol Size Distributions: Observations of Ultrafine Particle Events. *Aerosol Science and Technology*, *34*(1), 75-87. doi: 10.1080/02786820120056

Zilitinkevich, S., & Baklanov, A. (2002). Calculation Of The Height Of The Stable Boundary Layer In Practical Applications. *Boundary-Layer Meteorology*, *105*(3), 389–409. doi: 10.1023/A:1020376832738

Zilitinkevich, S., Baklanov, A., Rost, J., Smedman, A.-s., Lykosov, V., & Calanca, P. (2002). Diagnostic and prognostic equations for the depth of the stably stratified Ekman boundary layer. *Quarterly Journal of the Royal Meteorological Society*, *128*(579), 25–46. doi: 10.1256/00359000260498770

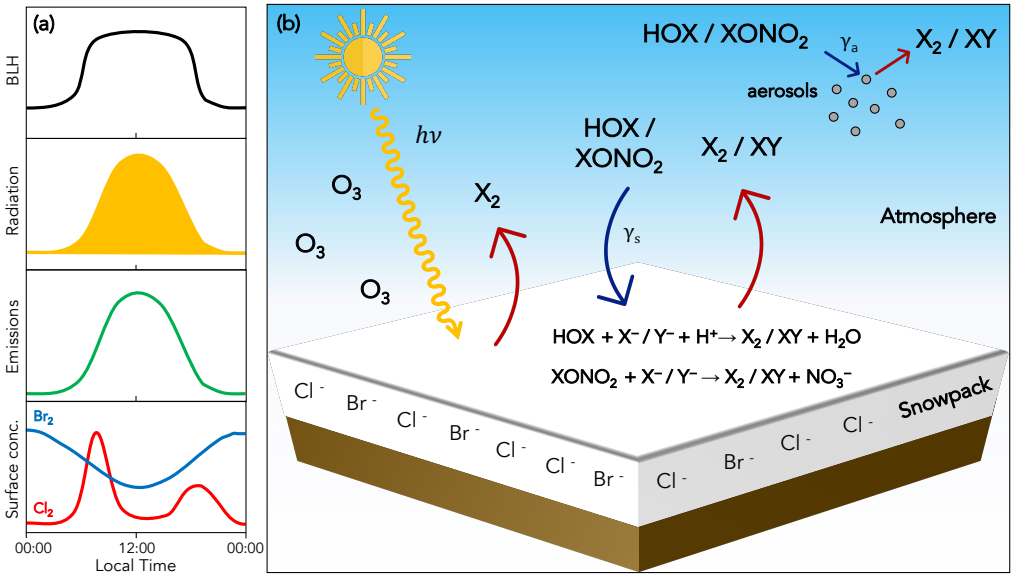

Figure 1. (a) Diurnal evolution of boundary layer height (BLH), solar radiation, chemical snowpack emissions, and surface concentrations of Cl_2 and Br_2 for an "average" day in the Arctic during spring (not drawn to scale). (b) Schematic of key polar halogen emissions from the continental snowpack (X = Cl, Br). Blue arrows represent loss processes and red arrows indicate production. Primary production of halogens is based on ozone and the availability of sunlight. Molecular halogens are also emitted via surface snow and aerosol recycling reactions, dependent on the heterogeneous reactive uptake coefficients γ_s and γ_a, on surface snow and aerosols, respectively.

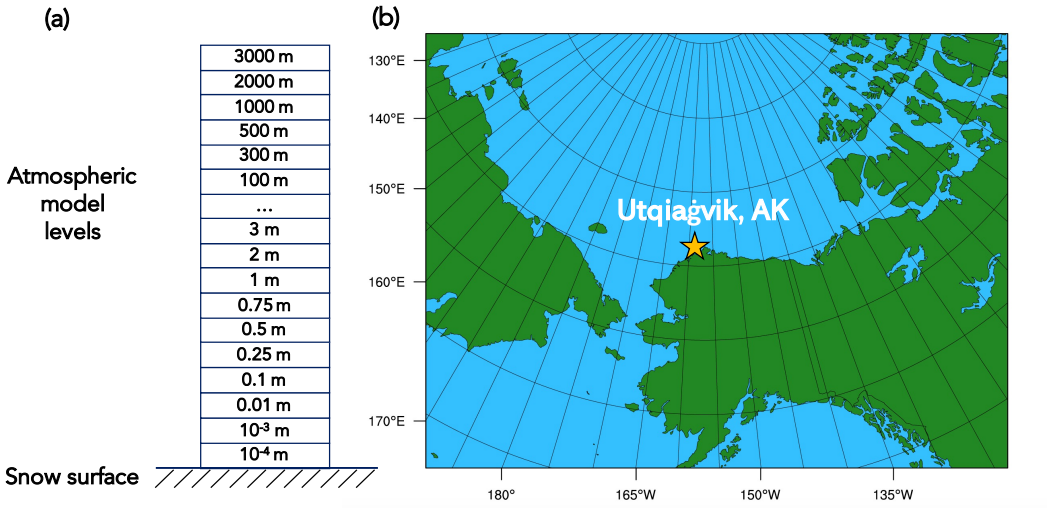

Figure 2. (a) PACT-1D model grid used with numbers representing the upper model level height in metres above the snow surface. (b) 3D WRF model domain centered on Utqiaġvik, Alaska.

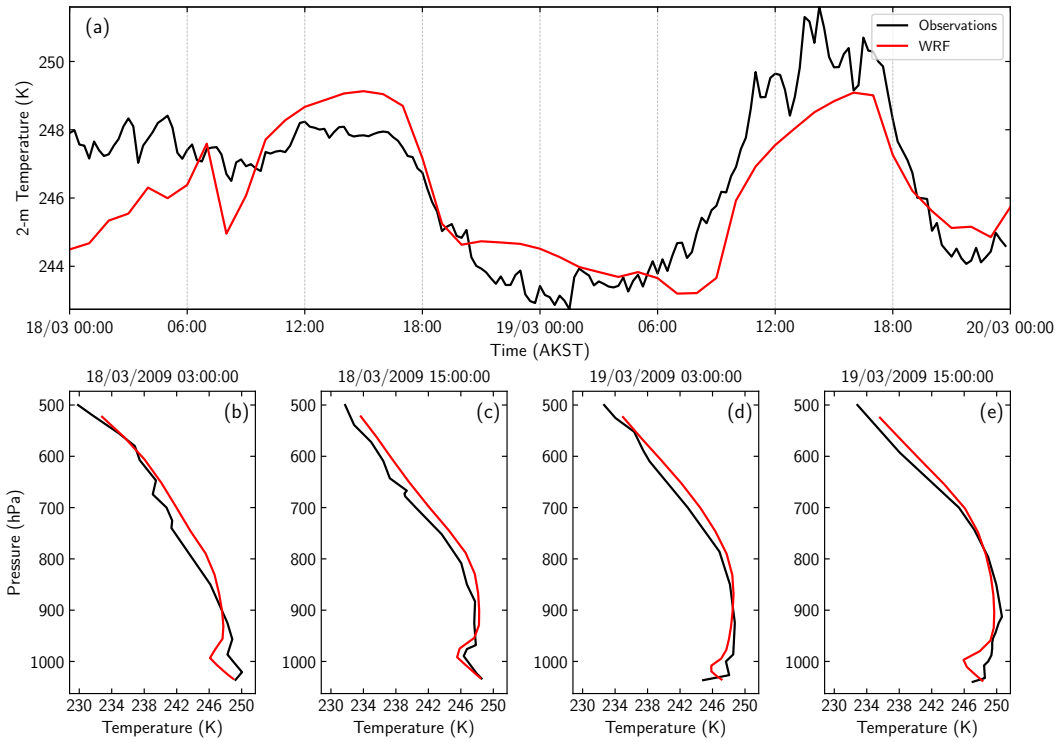

Figure 3. Temperature comparison between the WRF model (red) and measurements (black) at Utqiaġvik, Alaska during the simulation period. (a) 2-m temperature from WRF and surface measurements from OASIS. (b) - (e) Vertical temperature profiles from WRF and NOAA IGRA radiosondes released every 12 hours during the simulation period (dates and times are in Alaska standard time).

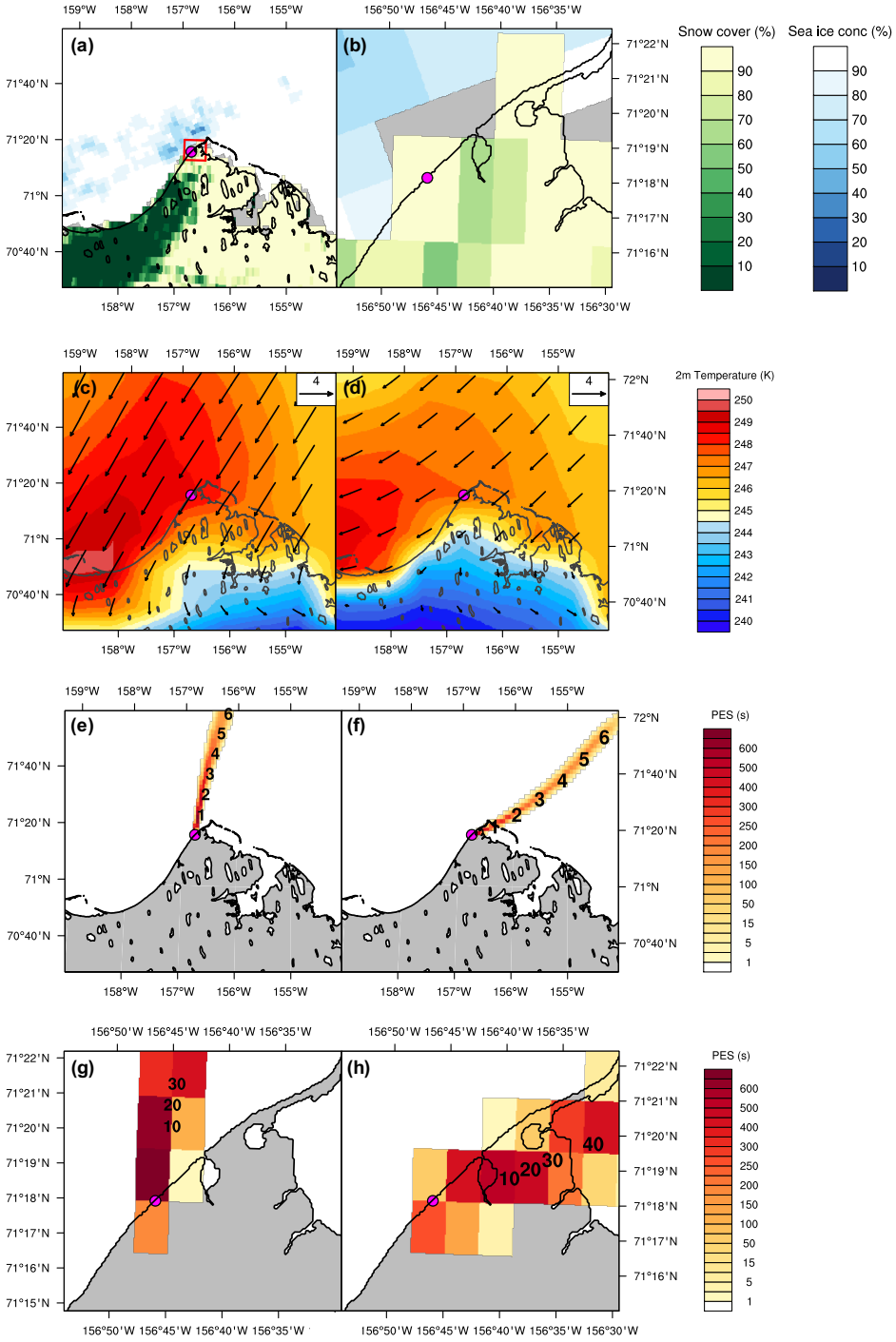

Figure 4. (a) AMSR-E satellite sea ice concentration and MODIS/Terra snow cover over Northern Alaska and (b) Utqiaġvik (marked in magenta) on 19/03/2009. Areas shaded in grey represent missing data. (c) 2-m temperature from WRF over Utqiaġivk at local noon on 18/03/09 and (d) 19/03/09 with 10-m wind speed and wind directions displayed as arrows. (e) FLEXPART-WRF 6-hour backwards surface (0-100 m) potential emission sensitivity (PES) over Northern Alaska on 18/03/09 – 09:00 AKST and (f) 19/03/09 – 18:00 AKST. Numbers represent hourly intervals since release. (g) and (h) Same as (e) and (f) respectively but for Utqiaġvik with numbers representing minute intervals since release.

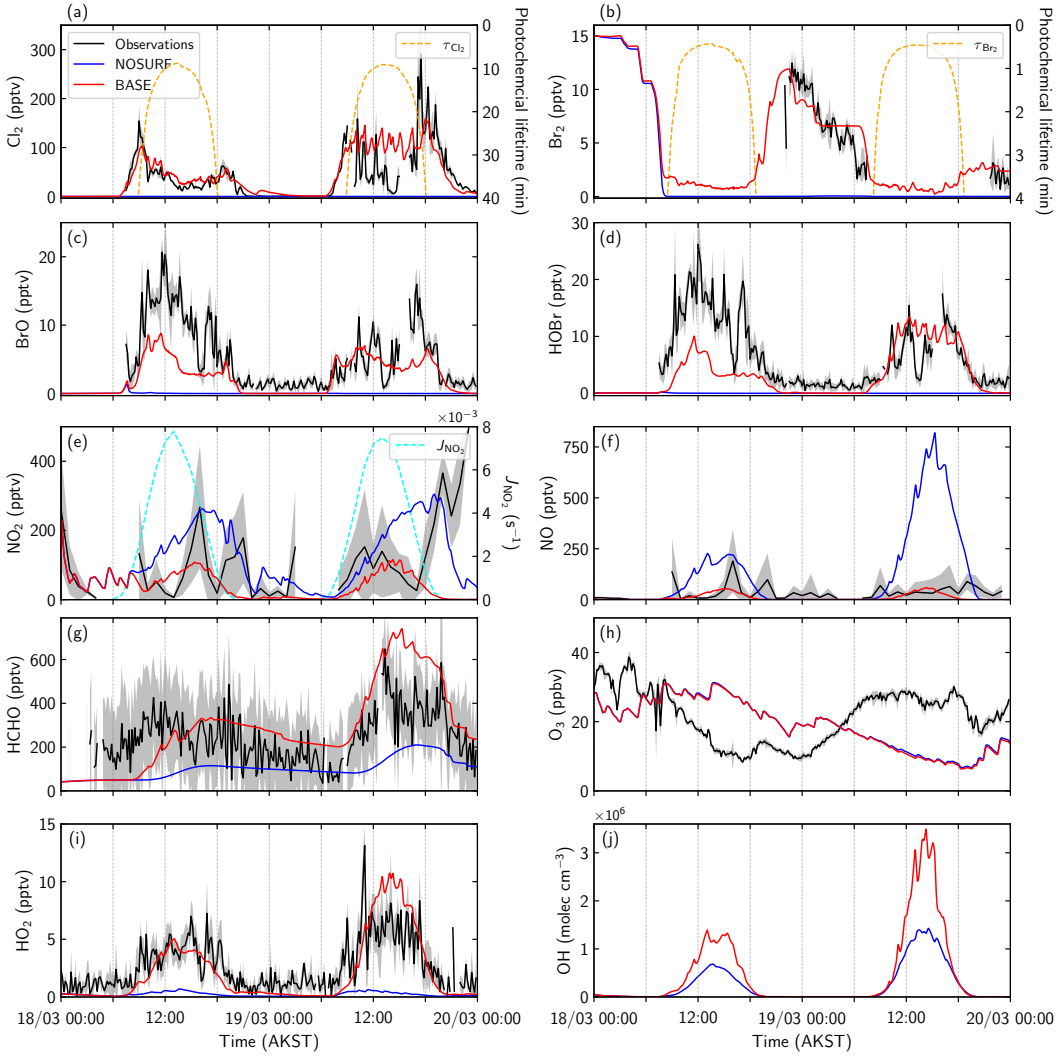

Figure 5. Model comparison with observations at 1.5 m above ground level during 18 and 19 March 2009. NOSURF (blue) and BASE (red) runs are compared with the 10-minute averaged measurements (black). NO_x measurements are plotted as an hourly average. Grey shaded areas represent the standard deviation of the average from the instantaneous measurements. Photochemical lifetimes of Cl_2 (τ_{Cl_2}) and Br_2 (τ_{Br_2}) (orange) and the calculated photolysis rate of NO_2 (J_{NO_2}) (cyan) are also plotted.

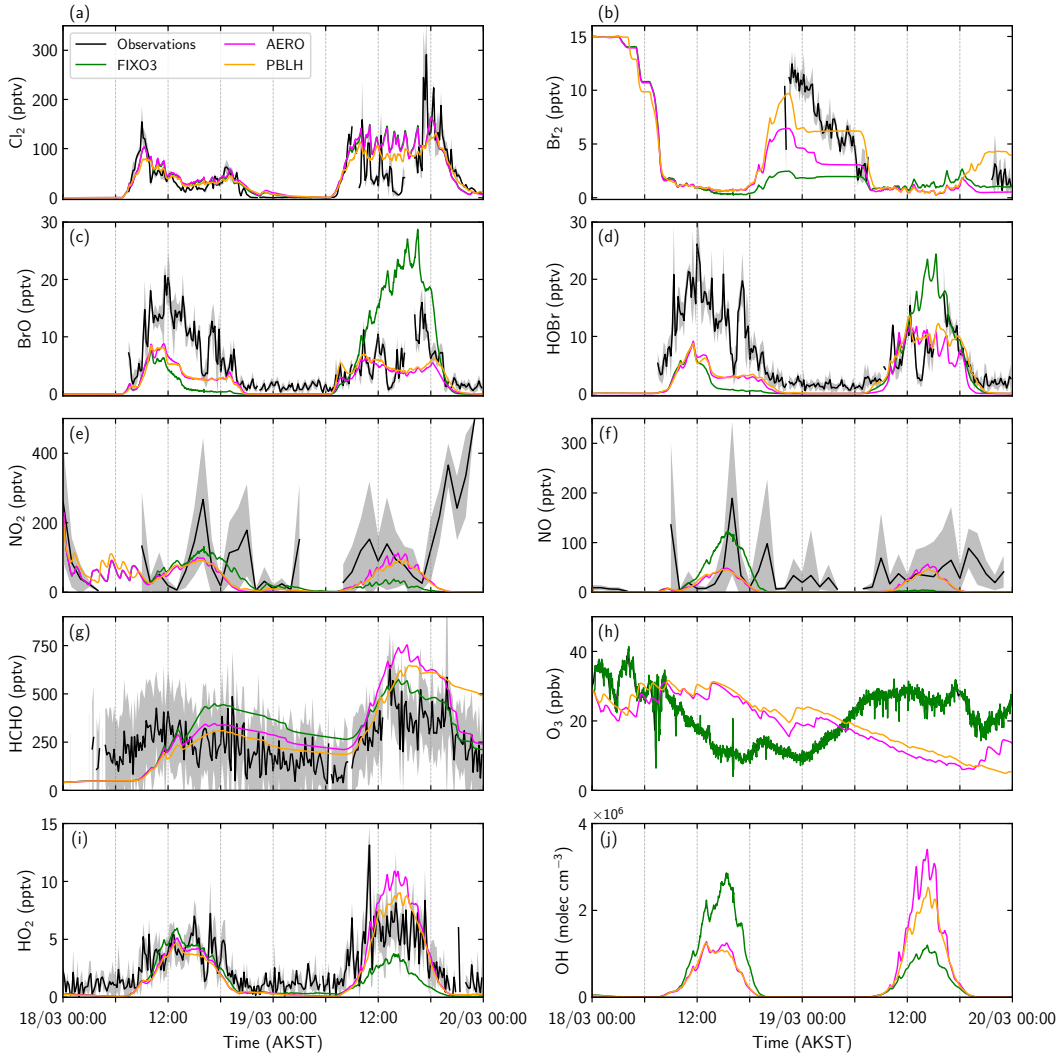

Figure 6. Model comparison of sensitivity runs with observations at 1.5 m above ground level during 18 and 19 March 2009. FIXO3 (green), AERO (magenta) and PBLH (orange) runs are compared with the 10-minute averaged measurements (black). NO_x measurements are plotted as an hourly average. Grey shaded areas represent the standard deviation of the average from the instantaneous measurements.

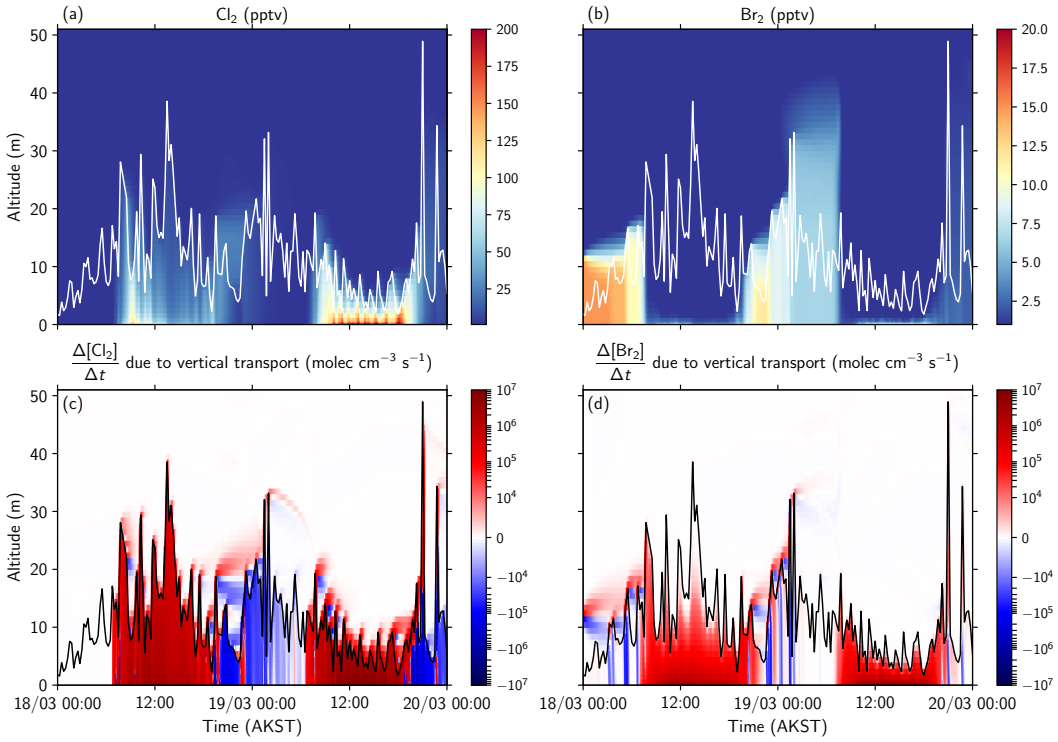

Figure 7. Modelled vertical distributions of (a) Cl_2 and (b) Br_2 during 18 and 19 March 2009 in the BASE run. White trace indicates the model prescribed surface inversion height. Modelled concentration change of (c) Cl_2 and (d) Br_2 due to vertical transport and deposition with respect to time. Black trace indicates the prescribed surface inversion height. Positive values represent upward transport and negative values indicate downward transport.

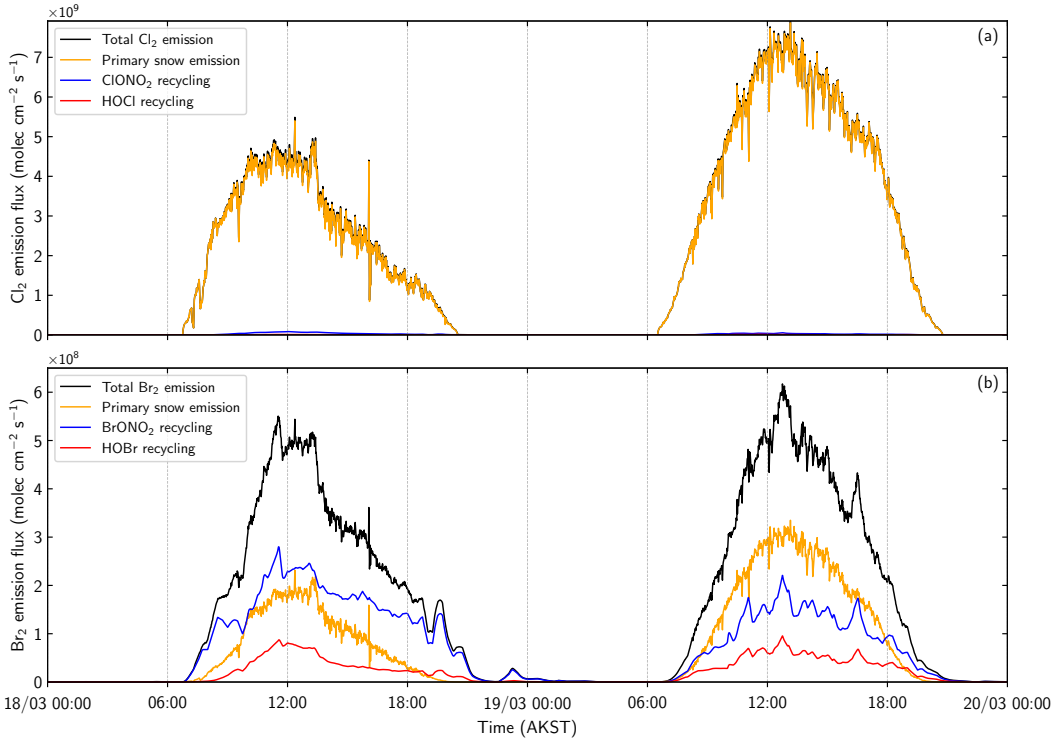

Figure 8. Snow emission and recycling fluxes of (a) Cl_2 and (b) Br_2 in the BASE run. The total emission flux (black) for each species is plotted together with the primary snow emission flux (orange) and recycling fluxes of $XONO_2$ (blue) and HOX (red), where X = Cl and Br.

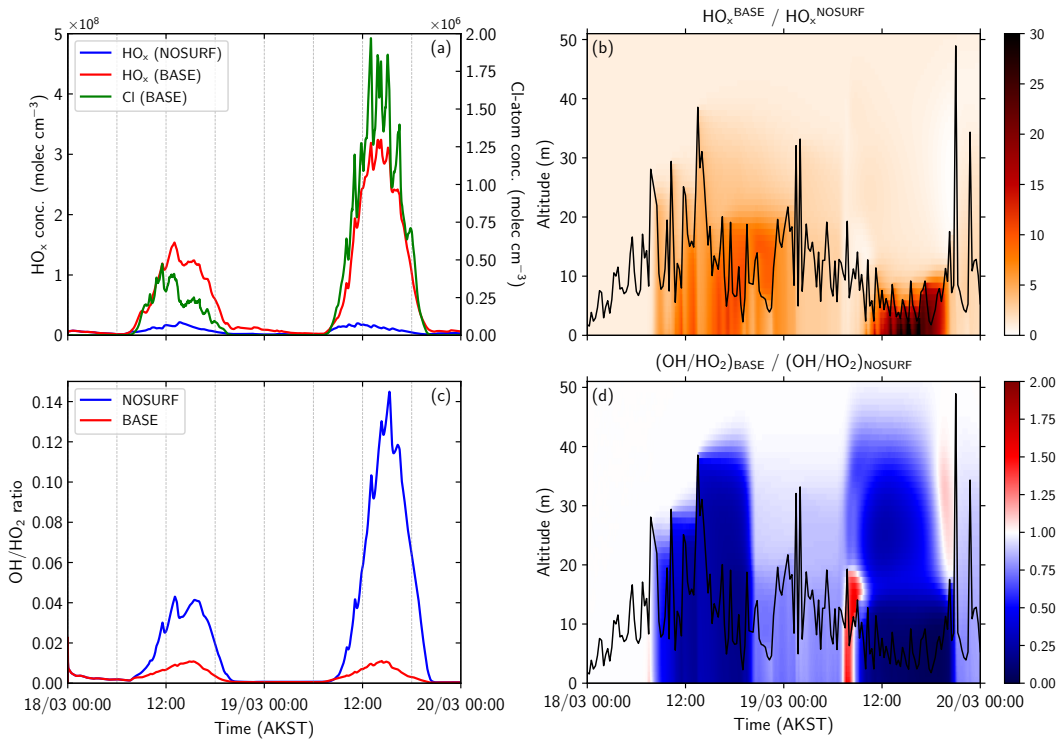

Figure 9. (a) Modelled HO_x concentrations at 1.5 m above ground level in the NOSURF (blue) and BASE (red) runs and Cl-atom concentration (green). (b) HO_x concentration in the BASE run divided by the HO_x concentration in the NOSURF run as a function of altitude. (c) OH/HO_2 ratio at 1.5 m above ground level in the NOSURF (blue) and BASE runs (red). (d) OH/HO_2 ratio in the BASE run divided by the OH/HO_2 ratio in the NOSURF run as a function of altitude.

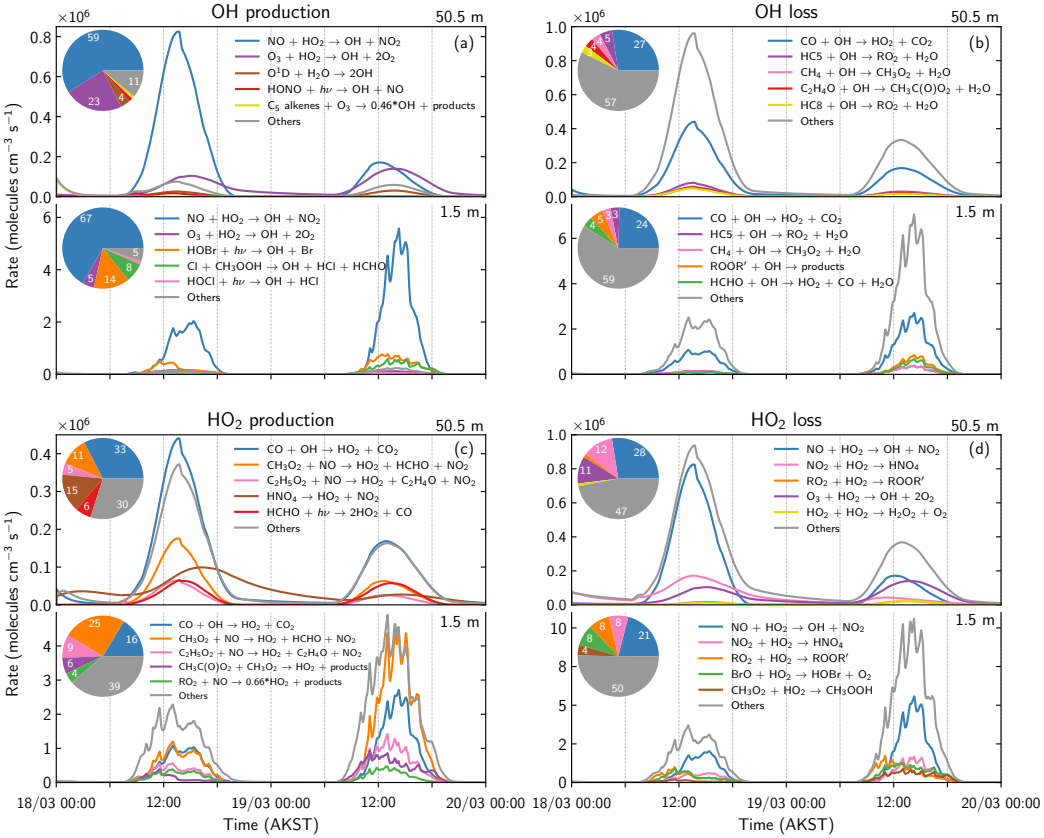

Figure 10. BASE simulation modelled (a) OH production (b) OH loss (c) HO_2 production, and (d) HO_2 loss each at 1.5 m and 50.5 m above the snow surface. The five largest contributing reactions are shown for each with the percentage contributions shown as a pie chart.

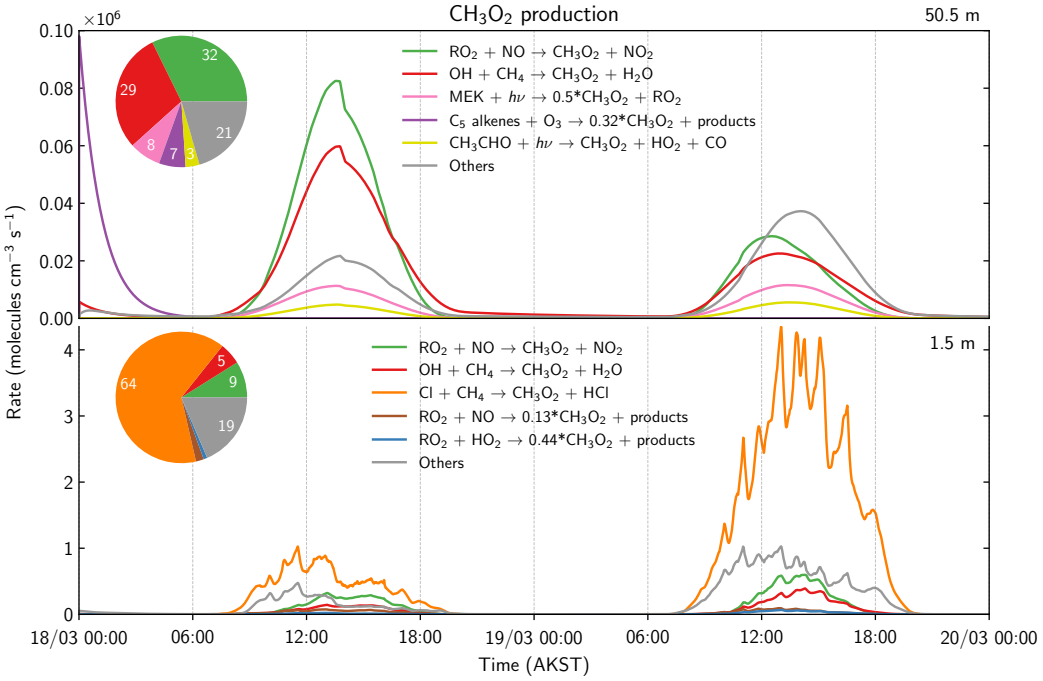

Figure 11. Modelled production reactions of CH_3O_2 at 1.5 m and 50.5 m above the snow surface. The five largest contributing reactions are shown for each with the percentage contributions shown as a pie chart.

Table 1. Measurements from the OASIS 2009 campaign used in this study.

Measurement	Method	Reference
Meteorology and turbulent fluxes	Ultrasonic anemometers	Boylan et al. (2014)
Cl_2, Br_2, BrO, HOBr	Chemical Ionization Mass Spectrometers (CIMS)	Liao et al. (2011, 2012, 2014)
OH, HO_2	Chemical Ionization Mass Spectrometers (CIMS)	Hornbrook et al. (2011), Mauldin III et al. (1998), Tanner et al. (1997)
NO, NO_2, O_3	Chemiluminescence	Helmig et al. (2012), Villena et al. (2011), Weinheimer et al. (1998)
HCHO	Difference Frequency Generation Tunable Diode Laser Absorption Spectrometer	Weibring et al. (2007, 2010)
CO	IR absorption CO analyzer	Parrish et al. (1994)
VOCs[a]	Trace Organic Gas Analyzer (TOGA)	Hornbrook et al. (2016)
Aerosol number density and radius	Optical Particle Counter (OPC) and Scanning Mobility Particle Sizers (SMPS)	Woo et al. (2001)
Actinic flux	CCD Actinic Flux Spectroradiometers (CAFS)	Shetter and Müller (1999)

[a]See Table 1 in Hornbrook et al. (2016)

Table 2. Heterogeneous reactions and reaction uptake coefficients on aerosols (γ_a).

Reaction	Heterogeneous reactive uptake (γ_a)	Reference
$HOCl + Cl^-_{(aq)} \rightarrow Cl_2$	2×10^{-4}	Ammann et al. (2013)
$HOCl + Br^-_{(aq)} \rightarrow BrCl$	2×10^{-4}	Ammann et al. (2013)
$ClONO_2 + Cl^-_{(aq)} \rightarrow Cl_2 + HNO_{3(aq)}$	0.03	Aguzzi and J. Rossi (1999)
$ClONO_2 + Br^-_{(aq)} \rightarrow BrCl + HNO_{3(aq)}$	0.05	Aguzzi and J. Rossi (1999)
$ClONO_2 \rightarrow HOCl + HNO_{3(aq)}$	0.03	Aguzzi and J. Rossi (1999)
$HOBr + Br^-_{(aq)} \rightarrow Br_2$	0.05	Pratte and Rossi (2006), IUPAC (2009)
$HOBr + Cl^-_{(aq)} \rightarrow BrCl$	0.05	Pratte and Rossi (2006), IUPAC (2009)
$BrONO_2 + Br^-_{(aq)} \rightarrow Br_2$	0.06	Deiber et al. (2004)
$BrONO_2 + Cl^-_{(aq)} \rightarrow BrCl$	0.04	Deiber et al. (2004)
$BrONO_2 \rightarrow HOBr + HNO_{3(aq)}$	0.04	Deiber et al. (2004)
$N_2O_5 + Cl^-_{(aq)} \rightarrow ClNO_2 + HNO_{3(aq)}$	0.02	Burkholder et al. (2019)
$N_2O_5 + Br^-_{(aq)} \rightarrow BrNO_2 + HNO_{3(aq)}$	0.011	Seisel et al. (1998)
$Cl_2 + Br^-_{(aq)} \rightarrow BrCl + Cl^-_{(aq)}$	0.2	Burkholder et al. (2019)
$OH + HCl \rightarrow 0.5 * Cl_2$	0.1	Knipping et al. (2000), Laskin et al. (2006)

Table 3. Description of the model runs performed in this study.

Model run	Description
NOSURF	Run with halogen snowpack emission routines deactivated.
BASE	Run with halogen snowpack emission and recycling routines active.
FIXO3	BASE run + O_3 fixed to the observations.
AERO	BASE run + heterogeneous recycling efficiency on aerosols increased by a factor of 10.
PBLH	BASE run + surface inversion height estimated using expression from Pollard et al. (1973).

Table 4. OH and Cl concentrations at 1.5 m and 50.5 m, at 12:00 AKST and 48-hour average in the NOSURF and BASE runs.

	1.5 metres		**50.5 metres**	
Species	12:00 AKST	48-hour average	12:00 AKST	48-hour average
	(molecules cm^{-3})		(molecules cm^{-3})	
$[OH]_{NOSURF}$	6.98×10^5	2.37×10^5	3.23×10^5	1.04×10^5
$[OH]_{BASE}$	1.22×10^6	4.57×10^5	3.21×10^5	1.04×10^5
$[Cl]_{BASE}$	7.19×10^5	2.65×10^5	22	7

Table 5. VOC lifetimes at 1.5 m and 50.5 m with respect to OH and Cl, at 12:00 AKST and 48-hour average in the NOSURF and BASE runs. Units h, d, and y represent time in hours, days, and years, respectively.

	12:00 AKST			48-hour average		
Species	τ_{OH}^{NOSURF}	τ_{OH}^{BASE}	τ_{Cl}^{BASE}	τ_{OH}^{NOSURF}	τ_{OH}^{BASE}	τ_{Cl}^{BASE}
1.5 metres						
HC3	9.7 d	5.5 d	2.8 h	28.5 d	14.8 d	7.5 h
HC5[a]	4.4 d	2.5 d	1.6 h	13.1 d	6.8 d	4.4 h
HC8[a]	1.8 d	1.0 d	1.1 h	5.2 d	2.7 d	3.0 h
Ethane	139 d	79.4 d	7.1 h	1.1 y	212 d	19.3 h
Ethene	1.7 d	23.4 h	2.0 h	5.0 d	2.6 d	5.3 h
Acetaldehyde	20.9 h	12.0 h	4.8 h	2.6 d	1.3 d	13.1 h
Acetone	112 d	64.0 d	11.6 d	329 d	171 d	31.9 d
MEK	15.9 d	9.1 d	9.2 h	46.9 d	24.3 d	1.0 d
Aldehydes ($\geq C_3$)	15.7 h	9.0 h	3.0 h	1.9 d	1.0 d	8.1 h
Toluene	2.2 d	1.2 d	6.5 h	6.4 d	3.3 d	17.8 h
50.5 metres						
HC3	20.8 d	20.9 d	10.3 y	64.6 d	64.6 d	32.4 y
HC5[a]	9.5 d	9.6 d	6.0 y	29.7 d	29.7 d	18.9 y
HC8[a]	3.8 d	3.9 d	4.2 y	11.9 d	11.9 d	13.1 y
Ethane	295 d	297 d	26.6 y	2.5 y	2.5 y	83.5 y
Ethene	3.7 d	3.7 d	7.4 y	11.5 d	11.5 d	23.1 y
Acetaldehyde	1.9 d	1.9 d	18.0 y	5.9 d	5.9 d	56.6 y
Acetone	241 d	243 d	1042 y	2.1 y	2.1 y	3275 y
MEK	34.4 d	34.6 d	34.2 y	107 d	107 d	108 y
Aldehydes ($\geq C_3$)	1.4 d	1.4 d	11.1 y	4.4 d	4.4 d	34.9 y
Toluene	4.7 d	4.8 d	24.4 y	14.7 d	14.7 d	76.8 y

[a]Reactions of HC5 and HC8 with Cl were not included in the chemical mechanism. We therefore calculate approximate chemical lifetimes using the rate constants of n-pentane and isopentane (in equal proportions) with Cl for HC5 and n-octane and iso-octane (in equal proportions) with Cl for HC8. Rate constants are obtained from Calvert et al. (2015) at 248 K.